

DEFORMATION MECHANISMS IN  
POLYCRYSTALLINE AGGREGATES  
OF MAGNESIUM

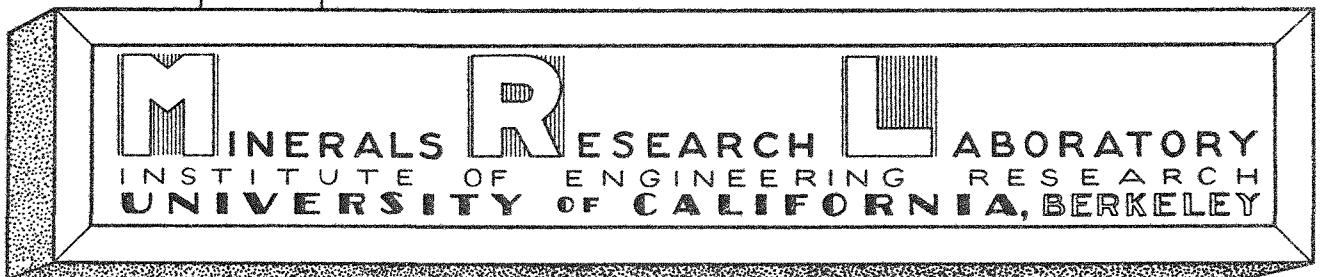
FIRST TECHNICAL REPORT

BY

F. E. HAUSER  
 C. D. STARR  
 L. S. TIETZ  
 J. E. DORN

MARCH 15, 1954

SERIES NO. 73 ISSUE NO. 2  
 TASK ORDER CONTRACT NO. 6  
 CONTRACT NO. DA-04-200-ORD-171



March 24, 1954

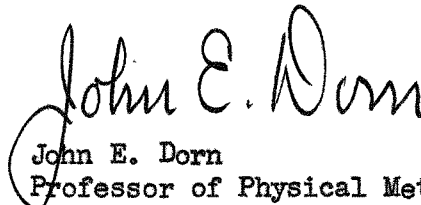
Commanding Officer  
Frankford Arsenal  
Bridesburg Station  
Philadelphia 37, Pennsylvania

ATTENTION: Mr. McCaughey

Dear Sirs:

Attached hereto are two copies of our First Technical Report on Task Order Contract No. 6, Contract No. DA-04-200-ORD-171, entitled "Deformation Mechanisms in Polycrystalline Aggregates of Magnesium". The significant observation made thus far centers about the low ductility and low fracture strengths of coarse-grained, high-purity magnesium. In the future investigations major effort will be devoted to elucidating the fracturing mechanisms and laws in polycrystalline aggregates of magnesium and its alloys as functions of grain size and temperature.

Sincerely yours,

  
John E. Dorn  
Professor of Physical Metallurgy

JED:dk

## **DISCLAIMER**

**This report was prepared as an account of work sponsored by an agency of the United States Government. Neither the United States Government nor any agency Thereof, nor any of their employees, makes any warranty, express or implied, or assumes any legal liability or responsibility for the accuracy, completeness, or usefulness of any information, apparatus, product, or process disclosed, or represents that its use would not infringe privately owned rights. Reference herein to any specific commercial product, process, or service by trade name, trademark, manufacturer, or otherwise does not necessarily constitute or imply its endorsement, recommendation, or favoring by the United States Government or any agency thereof. The views and opinions of authors expressed herein do not necessarily state or reflect those of the United States Government or any agency thereof.**

## **DISCLAIMER**

**Portions of this document may be illegible in electronic image products. Images are produced from the best available original document.**



Technical Report No. 1

DEFORMATION MECHANISMS IN POLYCRYSTALLINE

AGGREGATES OF MAGNESIUM

Technical Supervisor: Mr. McCaughey

Contractor:  
The Regents of the University of California  
Berkeley, California

Period Covered:  
1 June, 1953 to 1 March, 1954

Series 73, Issue 2  
Task Order Contract No. 6  
Contract No. DA-04-200-ORD-171

By

F. E. Hauser, C. D. Starr, L. Tietz and J. E. Dorn

## ABSTRACT

Deformation mechanisms in polycrystalline magnesium at atmospheric temperature were investigated by metallographic and X-ray techniques. Basal slip and twinning on  $(10\bar{1}2)$  planes were observed. In addition deformation took place by kinking and grain boundary shearing. Fracturing occurred on various crystallographic planes of high index as well as by an intergranular mechanism.

## INTRODUCTION

Scientific and technical interest have stimulated detailed and extensive investigations directed toward uncovering the fundamental processes involved in the plastic deformation of metals. The majority of such investigations have been concerned with simple stressing of single metal crystals with the objective in mind to simplify the analyses by eliminating many of the variables inherent in the more complex problem of deformation in polycrystalline aggregates; and the virtue of thus controlling and reducing the variables has been substantiated by the definitive correlations that have matured among the crystal structure, laws of deformation and the deformation mechanisms. But the ultimate objective of all such investigations has been the complete rationalization of the plastic behavior of polycrystalline aggregates. Whether the plastic behavior of polycrystalline aggregates might be completely deduced from singular knowledge of deformation mechanisms in single crystals has not yet been fully established. Undoubtedly the auxiliary knowledge gained from investigations on polycrystalline aggregates concerning the more general conditions of stressing encountered by each grain and concerning interactions at their mutual boundaries will be required before any extrapolation of the plastic properties of single metal crystals to those of the polycrystalline aggregate can be made with confidence.

The investigations described in this report were initiated as preliminary studies of deformation and fracture mechanisms in polycrystalline aggregates. It was thought that the polycrystalline aggregate would exhibit all of the mechanisms of deformation that could be detected in single metal crystals and that it might also reveal new mechanisms or new details of deformation processes fundamental to polycrystalline

behavior. High purity magnesium was chosen for this study not only because of the extensive interest in this light-weight metal but particularly because of the limited number of deformation mechanisms single crystals of magnesium are known to exhibit at atmospheric temperature. For this reason it appeared that polycrystalline magnesium would more readily exhibit new mechanisms of deformation and perhaps new details of deformation when deformed as a polycrystalline aggregate than metals from other systems that exhibit a greater number of deformation mechanisms.

The known fact that polycrystalline aggregates of magnesium undertake general plastic deformations suggests that each grain should exhibit at least five independent mechanisms of deformation. This conclusion follows from the argument that a general deformation involves six strain components; but the sum of the three normal components of the strain equals zero due to the fact that the volume remains constant; consequently only five independent mechanisms of deformation are required to account for the five independently variable components of the strain. The three mechanisms of basal slip can account for only two of the five required mechanisms, since all three are coplanar. The deformations arising from twinning in magnesium are negligible in view of its almost theoretical axial ratio for close packing. This suggests the possible introduction of pyramidal slip, which has been announced for single crystals particularly at elevated temperatures as necessary to account for the so-called three missing mechanisms of deformation; but, if pyramidal slip or other slip mechanisms are not found, yet other mechanisms of deformation will have to be uncovered to account for the facts.

### EXPERIMENTAL PROCEDURE

The preliminary objective of this investigation was to observe and evaluate the metallographic evidence following tensile straining of polycrystalline magnesium. A high purity magnesium extrusion was selected in preference to a casting in order to ensure better reproducibility of results and to provide for easier grain size control. It was recognized that this selection would not provide the most general observations since the extrusion would exhibit preferred grain orientations. Furthermore, by necessity, the observations would be limited to the surface grains. But it was hoped that such observations as could be made would nevertheless be somewhat indicative of the general behavior of internal grains as well.

High purity (99.97% Mg) magnesium was supplied by courtesy of The Dow Chemical Company in the form of extruded bars 0.100 inches thick and 0.75 inches wide. The bars were carefully machined into parallel gage section tension specimens 0.375 inches wide, having a gage length of 1.00 inch. The surface of each specimen was hand polished to remove the die markings and then given a grain coarsening anneal for 6 hours at 600°C in an SO<sub>2</sub> atmosphere. Following this each specimen was electrolytically polished in an ethyl alcohol solution containing 37.5% of orthophosphoric acid using 1.5 volts and 20 ma per dm<sup>2</sup>. Etching to reveal the grain boundaries was conducted in an aqueous solution containing 10% citric acid. The specimens exhibited a mean grain diameter of about 0.05 inches, deemed large enough to facilitate this initial study. Only a few excessively large grains were found in the gage section.

Five specimens were investigated in this study. Specimens 1, 2 and 5 were tested in the as-etched condition in order to review the general

characteristics of deformation. In order to provide a basis of local strain measurements and to assist in relocating interesting grains during interrupted tensile testing specimens 3 and 4 were lightly scribed with a ruling machine to produce a fine 0.0200 inches square grid over the gage section. Although some very small mechanical twins were produced in the immediate vicinity of the scribed lines by this procedure, the deformation observations were identical with those obtained on the ungridded specimens. Furthermore the orientations of 39 contiguous grains were determined in specimen 4 by microbeam back-reflection Laue X-ray technique, using Greninger's method of analysis, for the purpose of facilitating identifications of slip band markings, twin plane traces, crystallographically oriented low angle boundaries, fracture planes and mutual orientation effects in the vicinity of the grain boundaries.

Thirty-nine contiguous grains of specimen 4 were identified by the numbering scheme presented in Fig. 1. Fig. 2A illustrates the relative orientation of the tension axis of the specimen in each grain as viewed in terms of a standard projection. For the purpose of revealing more rapidly the type of preferred orientation encountered here, these same orientation data were plotted as a pole figure for the  $[0001]$  and the  $[11\bar{2}0]$  axes respectively as viewed with the net oriented parallel to the flat surface of the extruded bar (Fig. 2b). These data reveal that the predominating texture is one in which the basal plane lies in or near the extrusion plane with nearly equal scattering in all directions from this position while the  $[11\bar{2}0]$  slip directions are randomly oriented with respect to the extrusion direction. For purpose of discussion the orientation of each of the thirty nine grains was identified in terms of the angle  $\alpha$  between the tension axis and the  $[0001]$  direction and the angle  $\lambda$

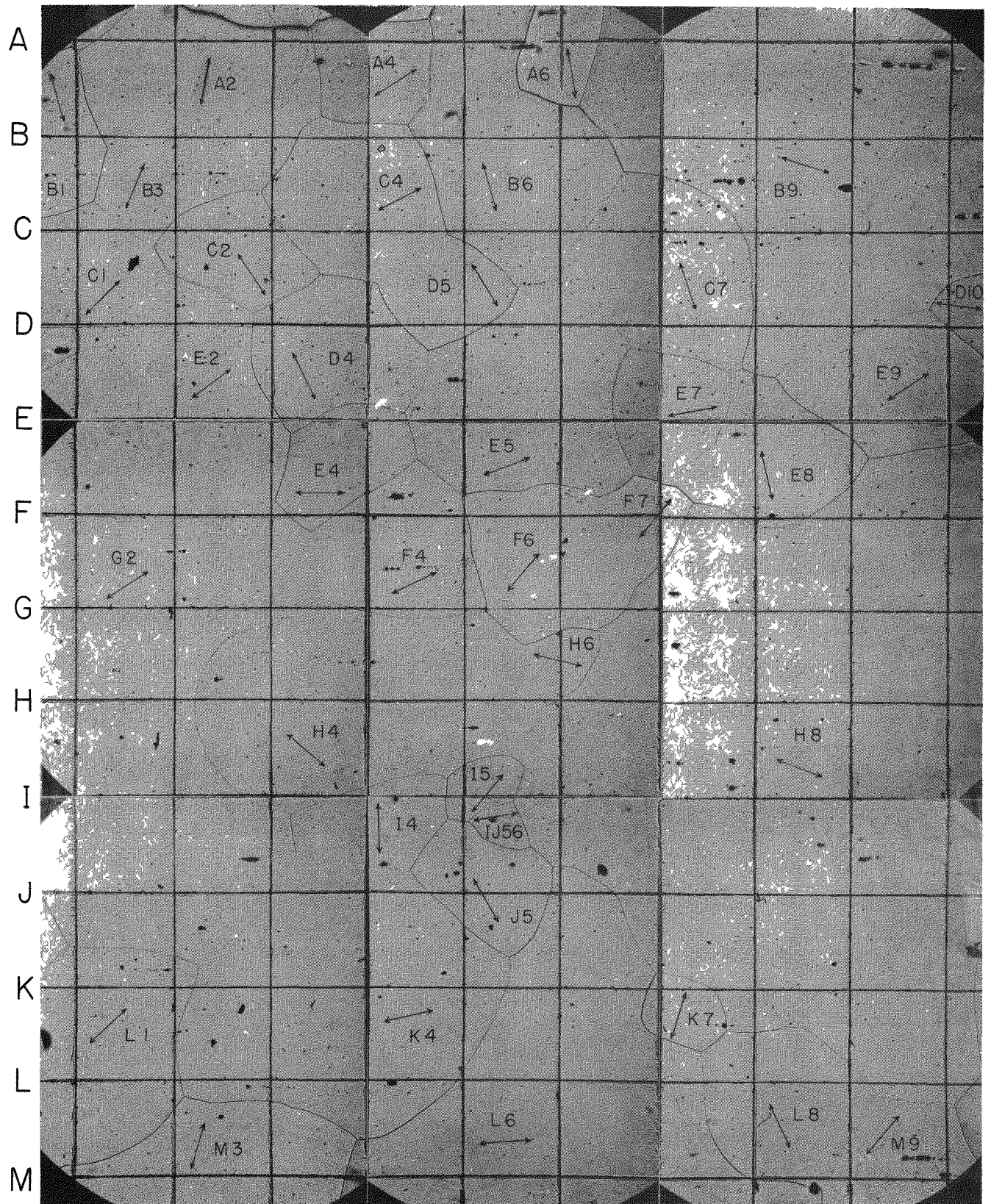


FIG 1 METHOD OF IDENTIFICATION OF GRAINS IN SPECIMEN 4. LINES REPRESENT SLIP DIRECTIONS CALCULATED FROM X-RAY ORIENTATIONS. SPECIMEN 4 AT 0%  $\epsilon$  (100X REDUCED BY 70%)

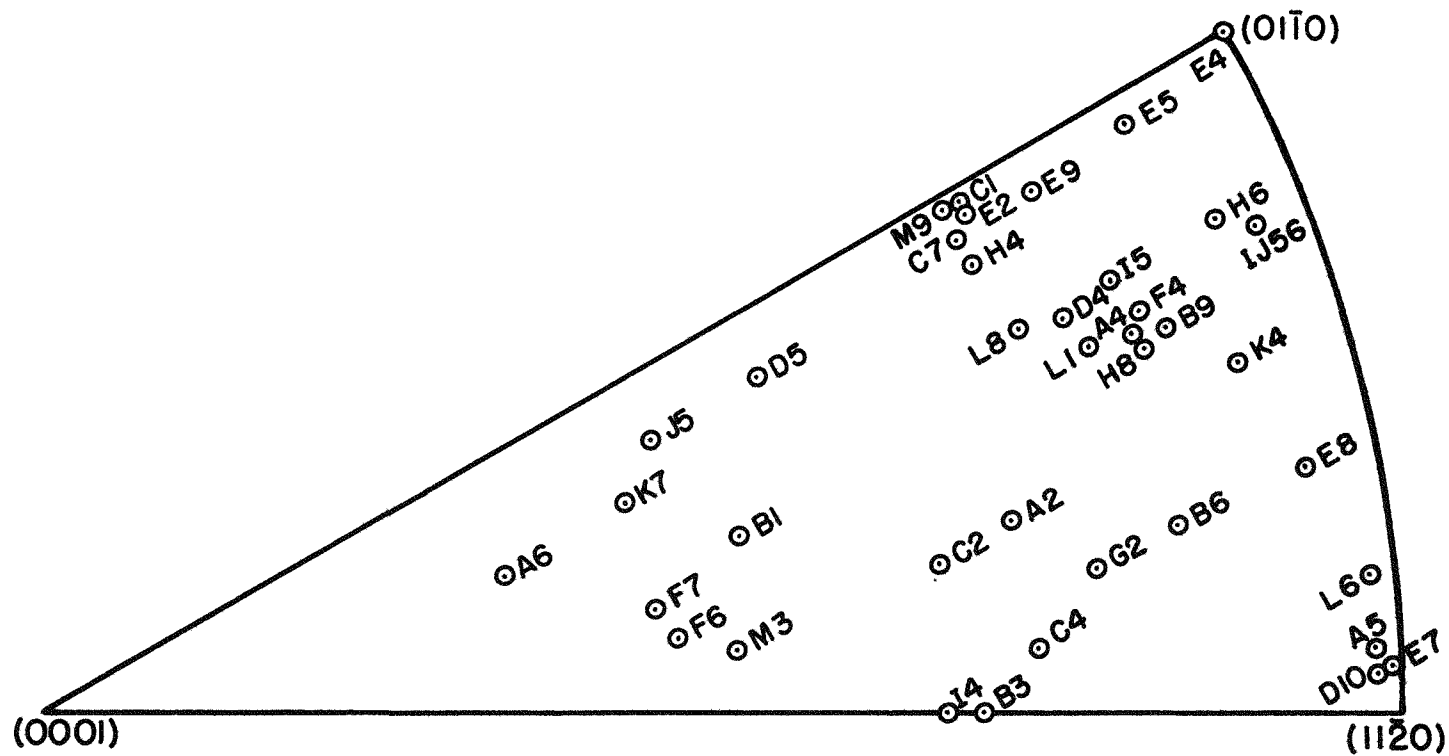


FIG. 2A ORIENTATION OF GRAINS IN SPECIMEN 4.  
 POLES OF TENSION AXIS OF EACH GRAIN REPRESENTED  
 ON STANDARD STEREOGRAPHIC PROJECTION.



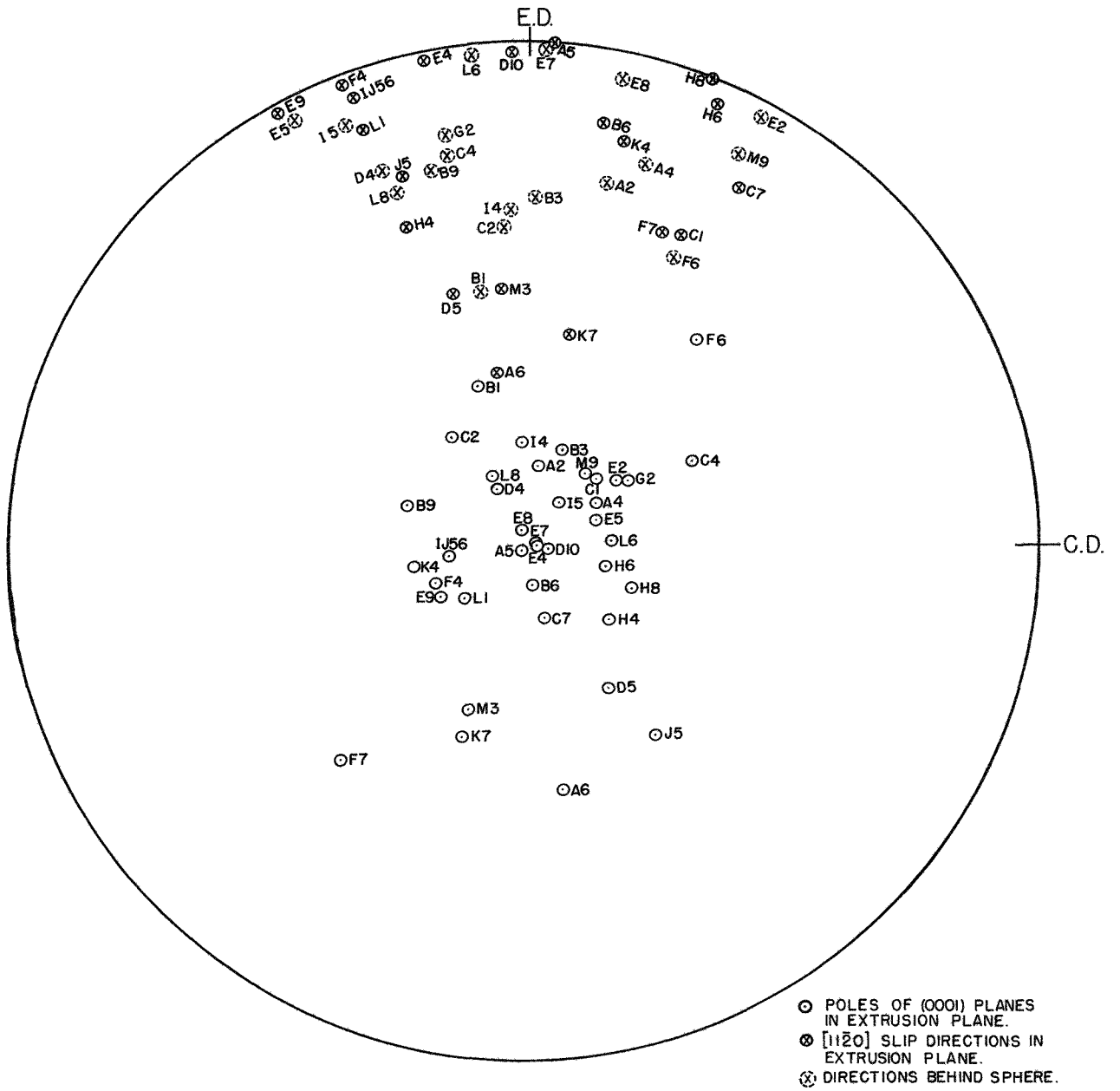


FIG. 2 b POLES OF (0001) AXES AND [11 $\bar{2}$ 0] DIRECTIONS  
 IN EXTRUSION PLANE.

between the tension axis and the most favorably oriented  $[11\bar{2}0]$  axis for basal slip as recorded in Table I. Thus the average shear stress  $\tau$  on the basal plane in the slip direction is

$$\tau = S \sin \alpha \cos \lambda$$

where  $S$  is the average tensile stress. Basal slip will therefore be facile on those grains having the largest values of  $\sin \alpha \cos \lambda$ . The data recorded in Table I reveal an extensive range of values of  $\sin \alpha \cos \lambda$  suggesting that the specimen contained grains of widely differing orientations.

### RESULTS AND DISCUSSION

As shown in Fig. 3, the tensile properties of the five specimens appeared to exhibit rather large scatter from each other. This, however, might partly be attributed to the limited number of grains in the section and occasional clustering, as shown by review of the data in Table I and Fig. 1, of grains of similar orientation. In addition specimens 1 and 5 were tested without interruption whereas specimens 2, 3 and 4 were unloaded periodically for removal from the tension testing machine for metallographic examination. As will be described more fully later, some twinning occurred during loading, but additional twinning was also observed to take place on unloading. Consequently both the interrupted testing and the resulting twinning might also have contributed to the scatter in the stress-strain curves for the various specimens. During the metallographic study on the tensile specimens the following observations were made.

Slip: All the slip-bands in each grain were parallel as shown by the typical photomicrograph in Fig. 4. Furthermore, the slip traces in all grains that exhibited slip in specimen 4 were in agreement with the

TABLE I

Orientation of Grains in Specimen 4

Grain	$\chi$	$\lambda$	Sin $\chi$ Cos $\lambda$
A2	18	21.5	.287
A4	9.5	21.5	.154
A5	1	3	.017
A6	51	53	.465
B1	34.5	37	.452
B3	21	21	.334
B6	9.5	13.5	.160
B9	8	20.5	.130
C1	15	53.5	.218
C2	22.5	24.5	.348
C4	17.5	18	.286
C7	17	36	.249
D4	13.5	21.5	.212
D5	30	38.5	.392
D10	1	2	.017
E2	15	34	.219
E4	0	12	.000
E5	6	32	.092
E7	0.5	2	.009
E8	3.5	11.5	.060
E9	11.5	34	.172
F4	8.5	22	.137
F6	40	40.5	.489
F7	41	42	.407
G2	14	16	.233
H4	16	30	.239
H6	4	23	.064
H8	9	21.5	.145
I4	23	23	.360
I5	9.5	24	.151
IJ56	2.5	22	.041
J5	38	44	.443
K4	5	17	.083
K7	41	45	.464
L1	12	22.5	.192
L6	1	6	.017
L8	15	26	.233
M3	36	36.5	.473
M9	16	34	.232

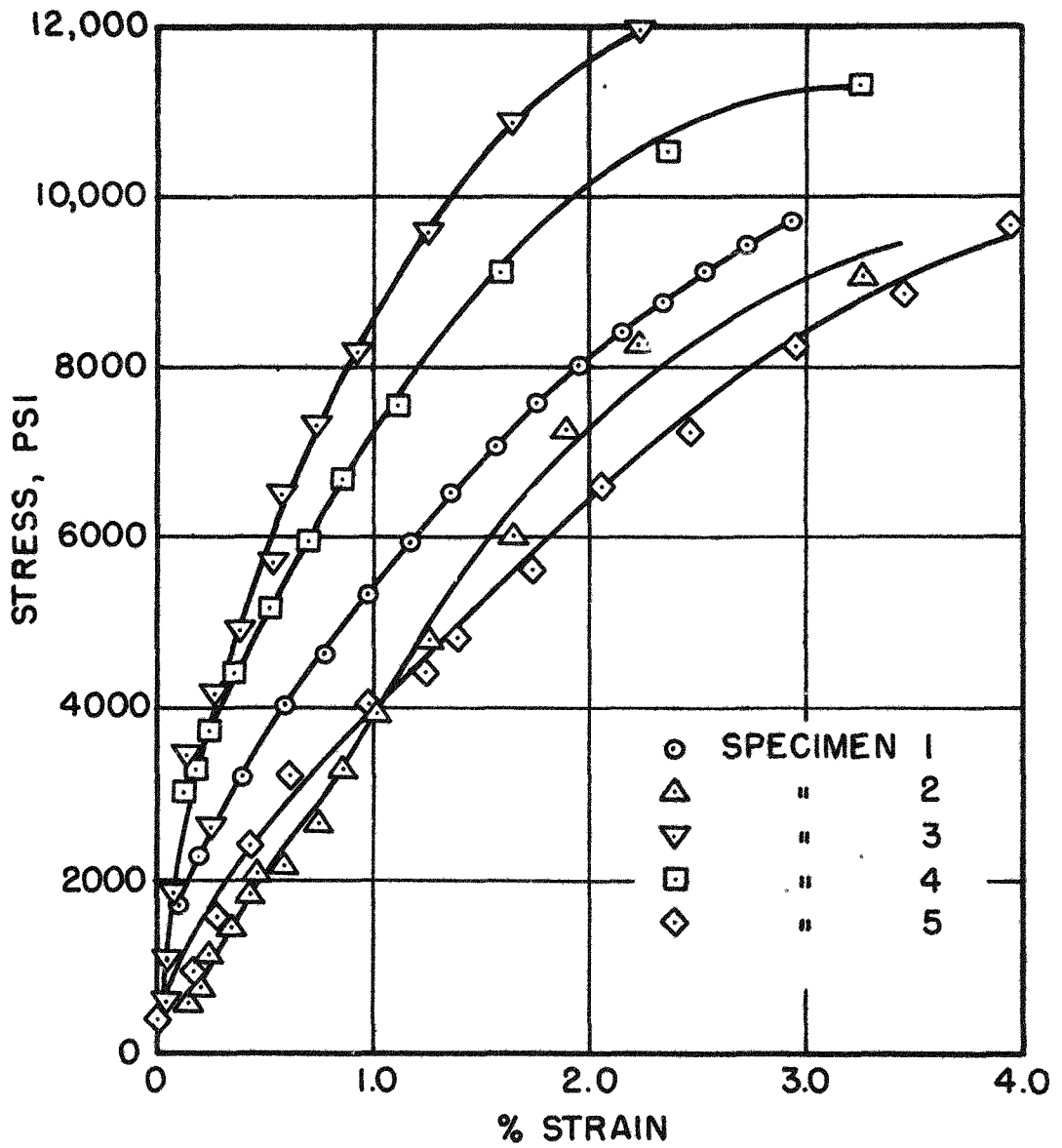


FIG. 3 STRESS-STRAIN CURVES FOR PURE MAGNESIUM AT ROOM TEMPERATURE. CURVES FOR SPECIMENS 2, 3, 4 PERIODICALLY INTERRUPTED FOR MICROSCOPICAL EXAMINATION.

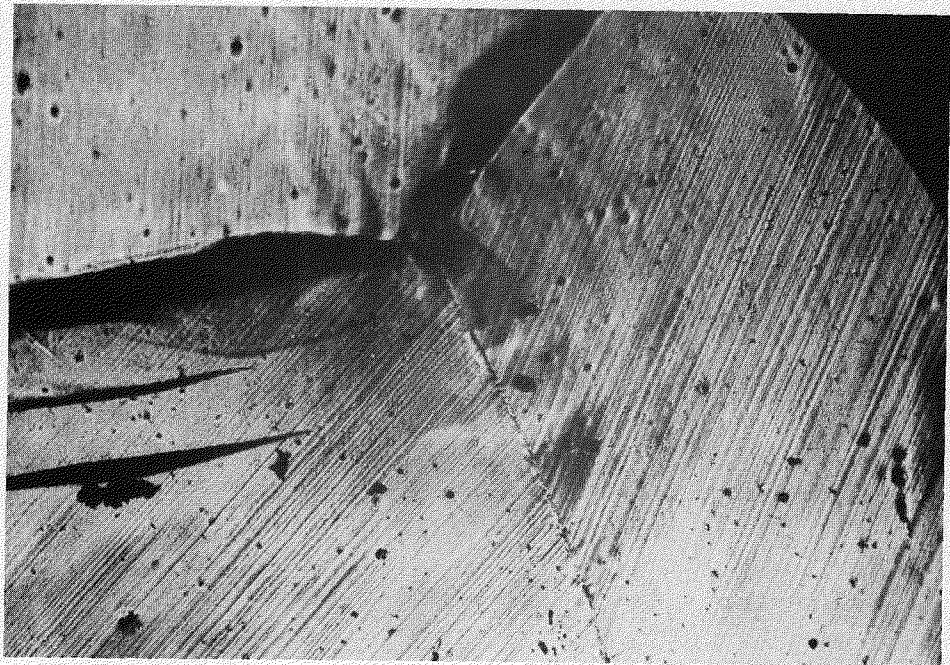


FIG. 4 BASAL SLIP IN PURE MAGNESIUM,  
SPECIMEN 2 AT 0.75%  $\epsilon$ , (100X)

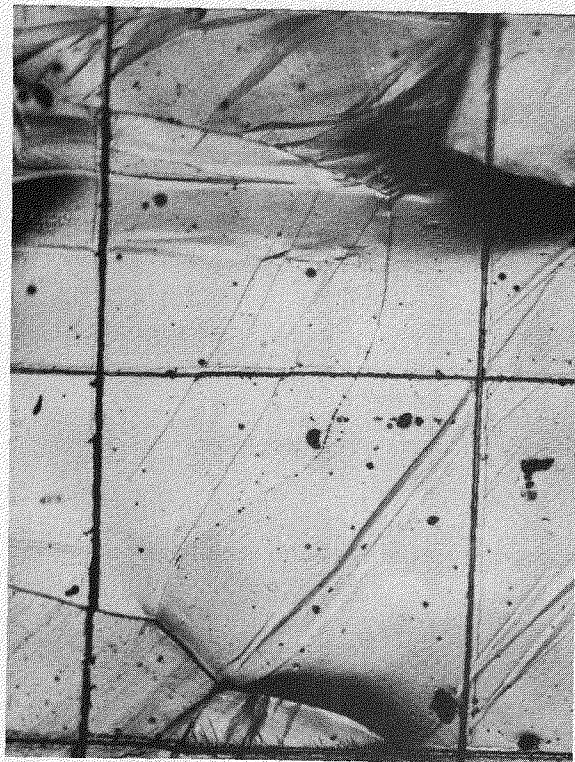


FIG. 5 FINE CRACKS IN SPECIMEN 4 ON  
GRAIN E7 AT 3.3%  $\epsilon$  (100X)

(0001)  $[11\bar{2}0]$  mechanisms given for single crystals of magnesium at low temperatures<sup>(1)</sup>. In specimens 2 and 3 where traces of twins and slip bands permitted an estimate of crystal orientation, slip was also observed to be consistent with the basal mechanisms (0001)  $[11\bar{2}0]$ . Basal slip was also evident in reoriented twin material. There was no evidence of duplex slip on two alternate sets of slip planes.

Grains A-5, D-10, E-4, E-5, E-7, H-6, I-J 5-6, and L-6 in specimen 4 (see Fig. 1) all had the basal plane almost parallel to stress direction. Since the resolved shear stress on the basal plane is very small, these grains were examined very closely for evidence of slip on pyramidal planes of the first type,  $(10\bar{1}1)$ . Although striations were observed on E-7 as shown in Fig. 5, they were identified as noncrystallographic cracks. No evidence was found that could be attributed to pyramidal slip. This is difficult to reconcile with the observation by Burke and Hibbard on single crystals of magnesium where faint striations were identified as traces of pyramidal slip planes<sup>(2)</sup>. They rationalized the advent of pyramidal slip at ambient temperature on the basis of grip constraint. Their observations seemed confirmed by additional data obtained by Dow Chemical Company during rolling of single crystals of magnesium<sup>(3)</sup>, wherein cross slip was observed in locally constrained areas. In this instance, however, the region which contained the second set of non-coplanar striations was so severely distorted that definite evaluation of the slip system must have been difficult. Since these striations were removed by re-etching, they were assumed to be slip traces and estimated to be evidence of pyramidal slip. Additional investigations on compression type specimens in which the basal planes were parallel to the stress direction, and which correspondingly produced a relatively high resolved shear stress on the  $(10\bar{1}1)$  planes, failed to exhibit pyramidal slip<sup>(4)</sup>.

Jillson<sup>(5)</sup> has questioned the interpretation of similar striations as evidence of pyramidal slip. Examination of basally cleaved surfaces of zinc single crystals which had been subjected to stretching and bending revealed, in addition to three sets of  $(10\bar{1}2)$  twin markings, three sets of striations, two of which were essentially normal and one parallel to the twin traces. Although the set of striations parallel to the twins might be ascribed to pyramidal slip, the two sets of striations normal to the twin traces cannot be accounted for by first order pyramidal slip. Instead it was suggested that all three sets of striations were the result of bending of the basal plane.

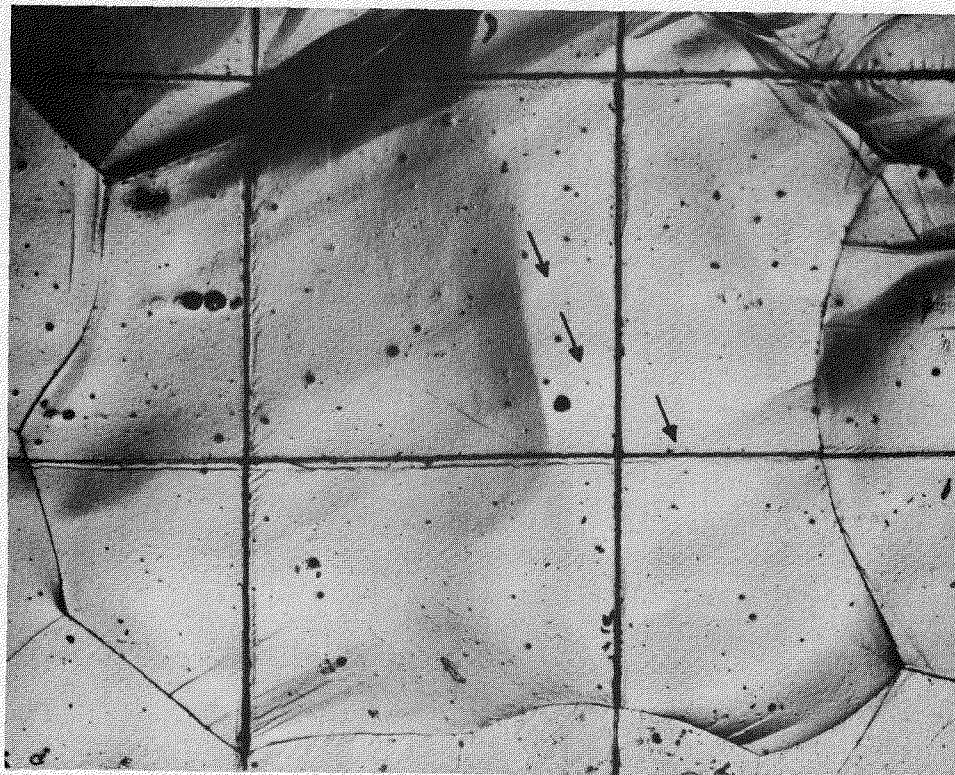
Examination of Grains E-5 and L-6 in specimen 4 reveals the presence of bend planes. Although the striations are somewhat curvilinear in grain E-5 as contrasted to the crystallographic marking in L-6 (shown in Fig. 6) both markings appear to correspond to traces from  $(10\bar{1}0)$  planes. These will be considered in more detail in a later section.

The advent of basal slip in single crystals has been shown to be stress dependent according to the relationship given in Eq. 1. The critical shear stress law for basal slip in magnesium is well established. Deviations from this law in polycrystalline aggregates might therefore be attributed to interactions between conjugate grains. The average resolved shear stress at which each grain was first observed to exhibit basal slip bands was estimated as recorded in Table II. Several factors, however, were involved in the accuracy of these estimations: First the observation of slip bands was done following each increment of tensile stressing (about 1000 psi). Secondly slip bands were detected by metallographic examination at 100 diameters. And thirdly slip was recorded only when several major slip bands were noted over the central section of the





(a) SPECIMEN 4, GRAIN L6 AT 2.4%  $\epsilon$  (100X)



(b) SPECIMEN 4, GRAIN E5 AT 2.4%  $\epsilon$  (100X)

FIG. 6 (10 $\bar{1}$ 0) BEND PLANES INDICATED BY  
ARROWS.



TABLE II

Critical Stress for Slip in Specimen 4

Grain	$\sin \chi$ $\cos \lambda$	Tensile Stress for Slip	Shear Stress for Slip
A2	.287	3,716	1066
A4	.154	7,544	1160
A5	.017	>11,300	---
A6	.465	3,013	1401
B1	.452	3,013	1362
B3	.334	3,013	1006
B6	.160	>11,300	---
B9	.130	5,952	774
C1	.218	3,261	711
C2	.348	3,716	1293
C4	.286	3,013	862
C7	.249	5,952	1482
D4	.212	5,952	1262
D5	.392	5,952	2333
D10	.017	>11,300	---
E2	.219	5,160	1130
E4	.000	>11,300	---
E5	.092	>11,300	---
E7	.009	>11,300	---
E8	.060	>11,300	---
E9	.172	5,952	1024
F4	.137	9,114	1250
F6	.489	5,160	2523
F7	.487	5,160	2510
G2	.233	3,261	760
H4	.239	3,261	779
H6	.064	3,261	209
H8	.145	5,160	748
I4	.360	5,160	1860
I5	.151	7,544	1140
IJ56	.041	9,114	374
J5	.443	3,013	1335
K4	.085	3,716	316
K7	.464	3,261	1513
L1	.192	5,160	991
L6	.017	>11,360	---
L8	.233	9,114	2120
M3	.473	3,013	1425
M9	.232	5,160	1200

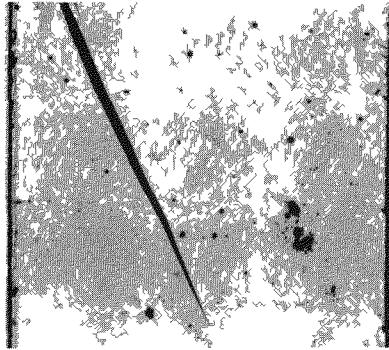
grain. This criterion was adopted because on occasions only one corner of a grain would exhibit a few early slip bands due to facile slip in the adjoining grains. The general trends of the data recorded in Table II support the thesis that favorably oriented grains begin to slip at lower tensile stresses than unfavorably oriented grains. On the other hand the resolved shear stress at which slip first became prominent exhibits considerable scatter from grain to grain. And although suspicion is prevalent that this scatter might arise from interactions between contiguous grains, a review of the data given in Tables I and II with the grain position identified in Fig. 1 suggests that the scatter is random.

Twinning: Mechanical twinning occurs in single crystals of magnesium on  $(10\bar{1}2)$  planes and is assumed to be the result of a simple shear in the  $[10\bar{1}1]$  direction plus minor atomic readjustments<sup>(6)</sup>. In the present investigation all twins formed on the  $(10\bar{1}2)$  planes. No evidence was found to corroborate twin formation on  $(10\bar{1}1)$  planes as reported on one occasion<sup>(7)</sup>.

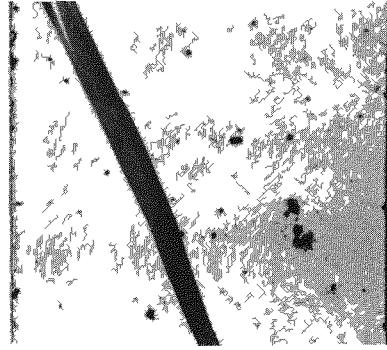
Microscopic examination revealed that twins grow in a uniform manner; bilaterally if no constraints are present or unilaterally in the presence of constraints as shown in Figs. 7A and B.

Magnesium may be detwinned by the application of a reverse stress as well as by residual stresses as postulated some years ago<sup>(8)</sup>. For example, the large twin present in Fig. 8 at an elongation of 0.52% has partially detwinned by subsequent straining to an elongation of 0.71%. Detwinning can also occur in cases where the twinned material has undertaken slip as shown in Fig. 9. Thus the original lattice is not necessarily restored to its initial conditions since visible microscopic features remain on the surface.

As shown in Fig. 10, as many as 5 different pyramidal planes eventually became active twin planes in one grain (M-3). Although it is

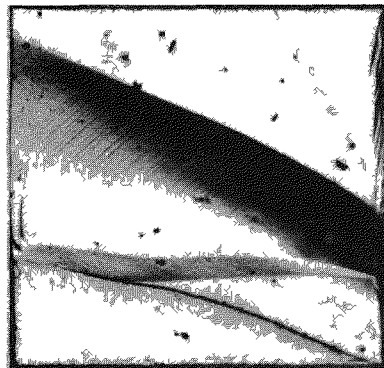


1.1 %  $\epsilon$

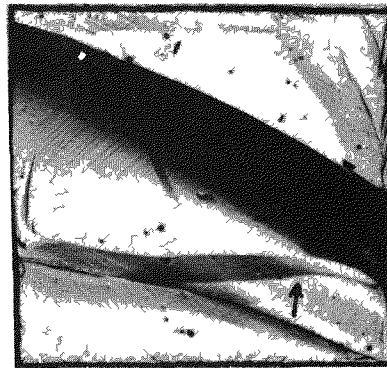


1.6 %  $\epsilon$

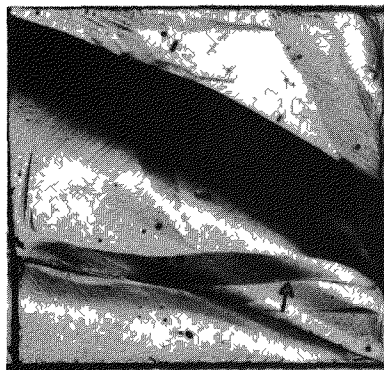
FIG. 7a BILATERAL TWIN GROWTH  
SPECIMEN 4 (100X)



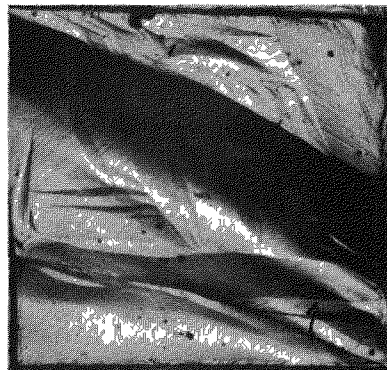
0.25 %  $\epsilon$



0.52 %  $\epsilon$

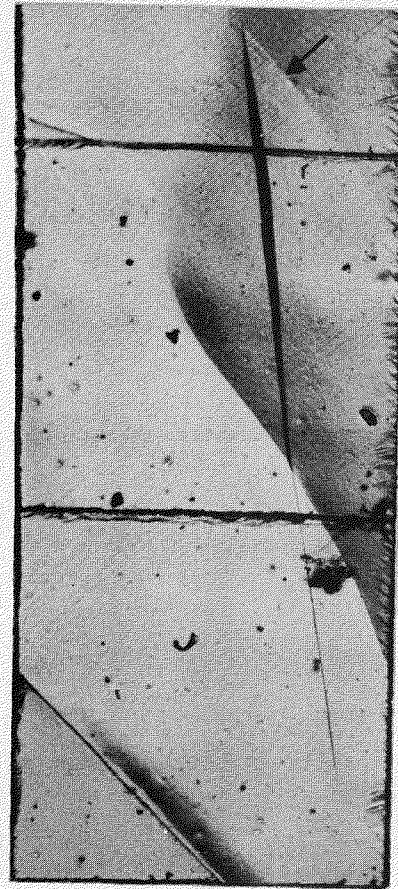


0.71 %  $\epsilon$

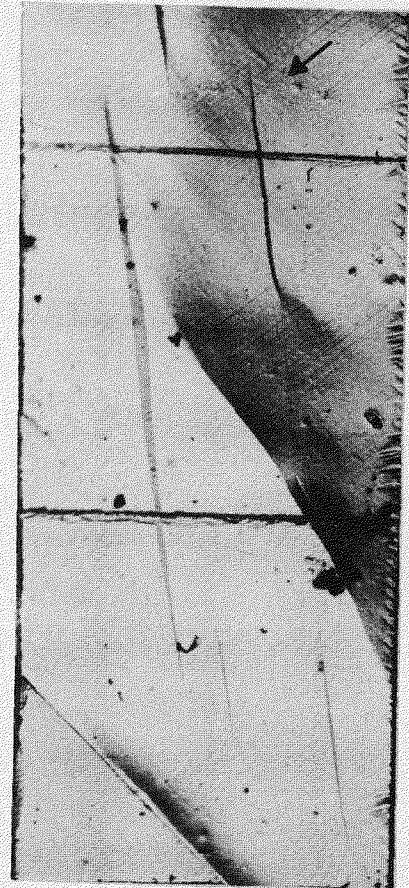


1.1 %  $\epsilon$

FIG. 7b UNILATERAL TWIN GROWTH  
IN PRESENCE OF CONSTRAINTS.  
SPECIMEN 4 (100X)



0.52 %  $\epsilon$



0.71 %  $\epsilon$

FIG. 8 DETWINNING DURING TENSILE STRAINING OF MAGNESIUM. NOTE THAT LOW ANGLE BOUNDARY ALSO DISAPPEARS. SPECIMEN 4. (100X).

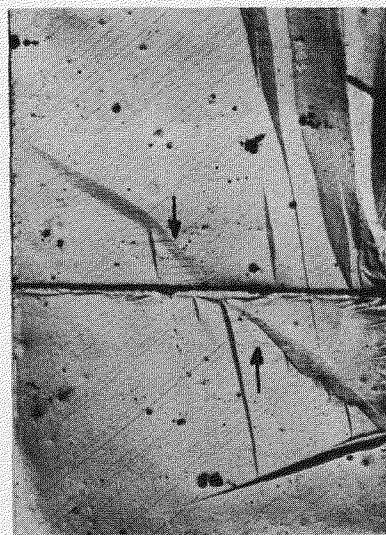


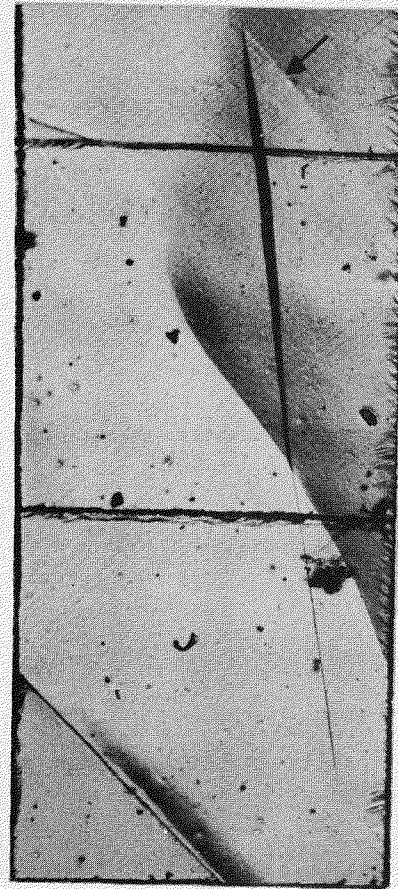
FIG. 9 SLIP TRACES REMAINING ON SURFACE AFTER DETWINNING. SPECIMEN 4 AT 0.52 %  $\epsilon$ . (100X).



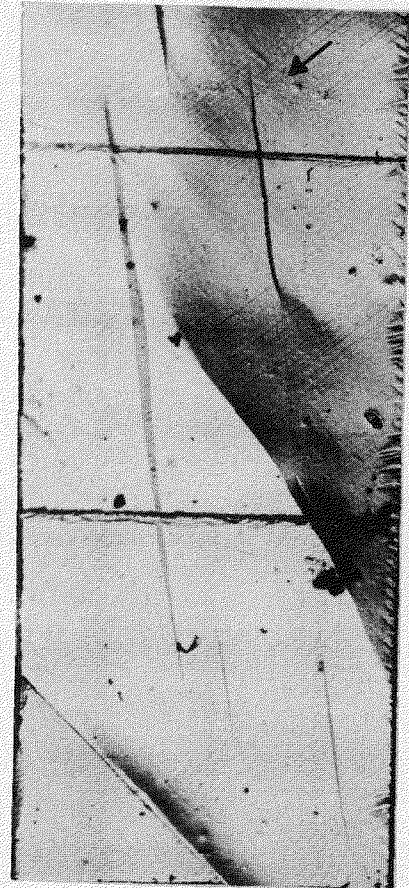


FIG. 10 FIVE OPERATIVE TWIN MECHANISMS IN GRAIN M3  
OF SPECIMEN 4 AT 0.25 %  $\epsilon$ . (100X REDUCED BY 20%)





0.52 %  $\epsilon$



0.71 %  $\epsilon$

FIG. 8 DETWINNING DURING TENSILE STRAINING OF MAGNESIUM. NOTE THAT LOW ANGLE BOUNDARY ALSO DISAPPEARS. SPECIMEN 4. (100X).

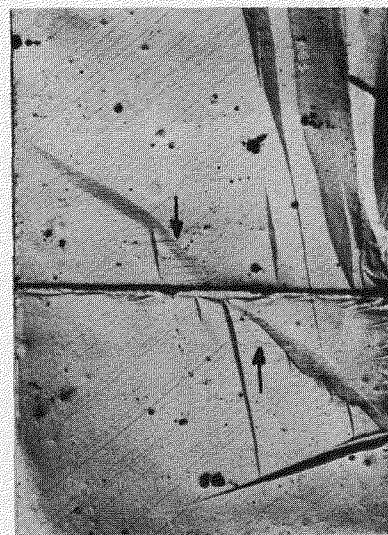


FIG. 9 SLIP TRACES REMAINING ON SURFACE AFTER DETWINNING. SPECIMEN 4 AT 0.52 %  $\epsilon$ . (100X).





FIG. 10 FIVE OPERATIVE TWIN MECHANISMS IN GRAIN M3  
OF SPECIMEN 4 AT 0.25 %  $\epsilon$ . (100X REDUCED BY 20%)

possible for all six pyramidal planes to be active, only select orientations as shown in Fig. 11<sup>(8)</sup> might exhibit these mechanisms for uniaxial tensile stresses. But as shown in Fig. 11, Grain M-3 lies in region C and should therefore exhibit only 2 mechanisms of twinning during tensile straining instead of the 5 observed. Furthermore all grains oriented in region D would exhibit contraction in the direction of tensile straining if twins were formed. The large number of twins present in grains such as H-8 in Fig. 12 which should not exhibit twinning during tensile straining suggest that either the operative stress direction in polycrystalline aggregates must be vastly altered or twins were formed during the periodic unloading of the specimen for metallographic examination. Measurement of the distance between grid lines also revealed that the grains had actually contracted in the tensile direction. Subsequent uninterrupted tensile stressing of specimen 5 revealed 33 twins in 29 grains of known orientation at 3.3% elongation. During the tensile test at constant strain rate 10 twins caused extension while 23 twins produced contraction in the stress direction. Thus the overall strain due to twinning in this specimen is actually negative, a fact not easily reconciled with strain energy considerations.

It has been suggested that twinning is a shear stress dependent phenomenon although the evidence is not at all conclusive<sup>(9-10)</sup>. Instead, numerous observations suggest that twinning is the result of a more complex mode of deformation arising from concurrent bending and stressing.<sup>(2,7,11)</sup> For example, irrespective of crystal orientation, Burke and Hibbard<sup>(2)</sup> observed that twins were formed in single crystals of magnesium only near the grips or adjacent to cemented wire strain gages when external constraints were present. Since both the grips and strain gages restrain



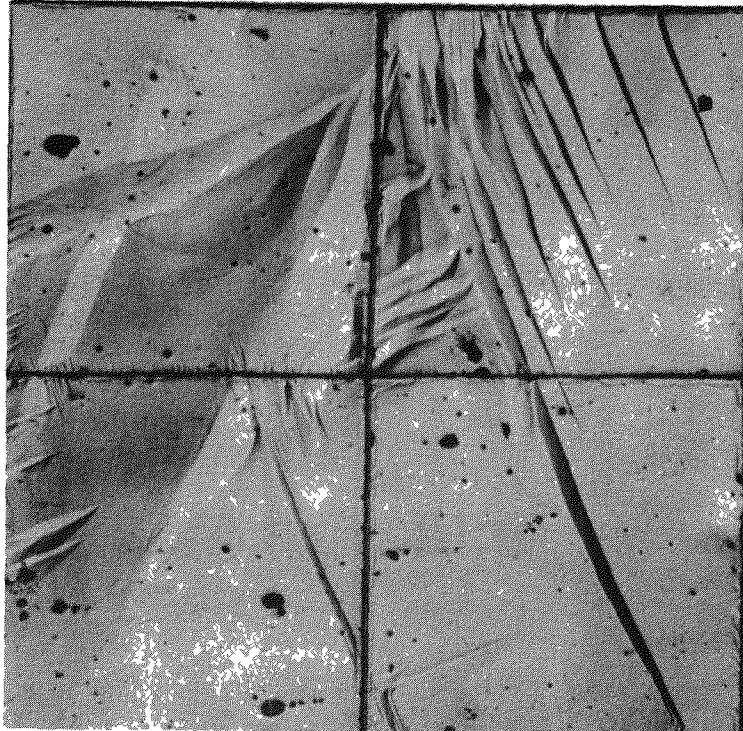


FIG. 12 ABUNDANT TWIN FORMATION IN  
GRAIN H8 OF SPECIMEN 4 AT 2.4 %  $\epsilon$ .  
TWINNING ON ALL  $(10\bar{1}2)$  PLANES CAUSES  
CONTRACTION IN TENSILE DIRECTION (100X)

the rotation of the slip plane during tensile straining, it was suggested that some phenomenon such as bending existed in conformity with the applied stress to produce twinning. This suggestion appeared justified by the observation that the size and number of twins decreased as the amount of bending decreased. Additional corroboration is afforded by the observations of Bakarian<sup>(12)</sup> that magnesium, regardless of initial orientation, will twin readily when suddenly twisted or bent.

### BENDING PLANES ASSOCIATED WITH TWINNING

#### A. Bending Preceding Twinning

Although the twinning system for magnesium is recorded as  $(10\bar{1}2)$   $[10\bar{1}1]$ , no atomic movements by simple shear have been found which will permit twinning without distortion. In addition to the conventional simple shear, secondary adjustments at right angles to the twinning direction are necessary for the atomistic process of twinning. It has been suggested that this secondary adjustment could be achieved by a bending on a  $(11\bar{2}0)$  plane prior to twin formation<sup>(2)</sup>. Microscopic evidence of the termination of twins at traces of  $(11\bar{2}0)$  planes appear to substantiate this hypothesis. Similar striations described as bend planes about a  $[10\bar{1}0]$  axis have been recorded for zinc<sup>(5)</sup>. Careful examination of the grains which exhibited twinning in the present investigations, however, failed to reveal any bending of the basal plane about the  $[11\bar{2}0]$  axis.

#### B. Bending Accomodating Twinning

The process of twinning also results in a decided bending of the basal plane as shown by Jillson's schematic diagram given in Fig. 13. This phenomenon has been termed an accomodation plane or band<sup>(5)</sup>, accomodation kink<sup>(13)</sup>, and crystallographic low angle boundary.<sup>(14)</sup> Numerous such

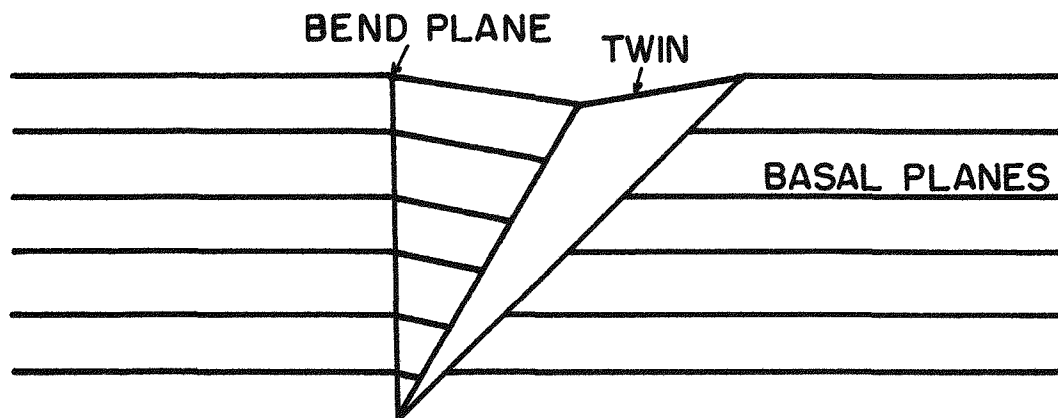
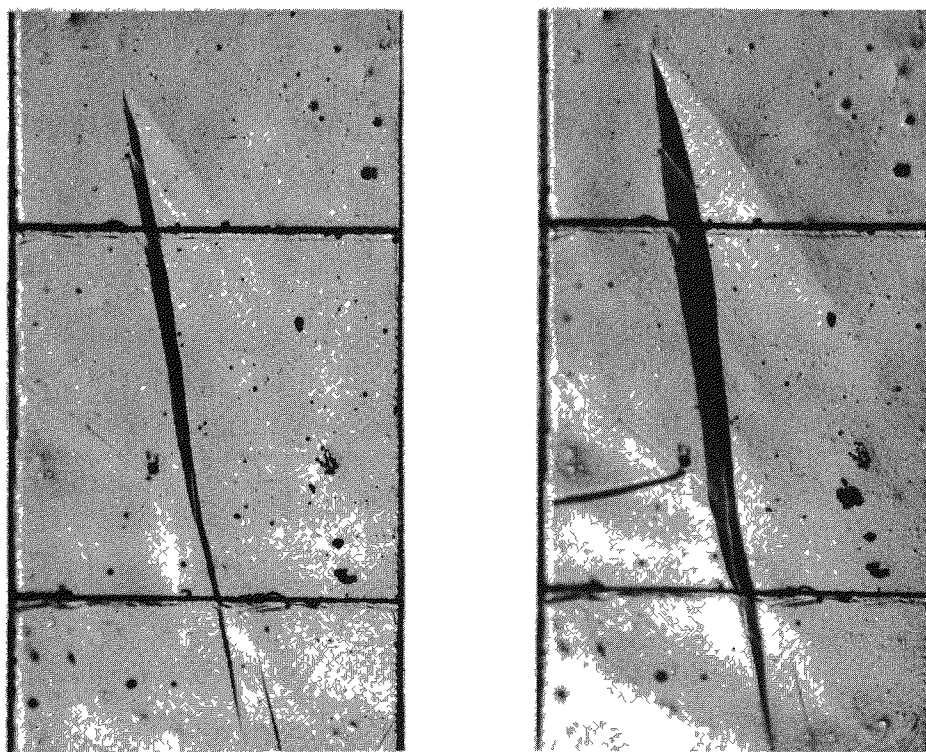


FIG. 13 SCHEMATIC ILLUSTRATION OF BEND PLANE ASSOCIATED WITH FORMATION OF A TWIN.  
(AFTER JILLSON<sup>5</sup>)



(a) 1.1 %  $\epsilon$

(b) 1.6 %  $\epsilon$

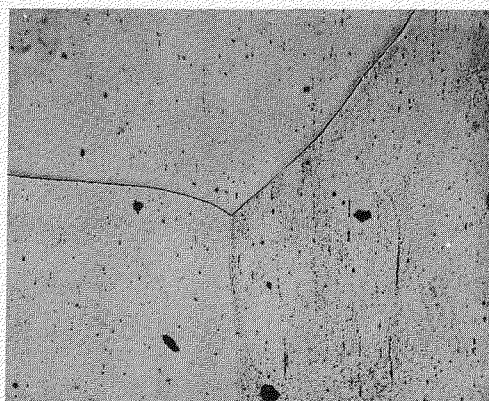
FIG. 14 LOW ANGLE ACCOMODATION BOUNDARY ACCOMPANYING GROWING TWIN. SPECIMEN 4 (100X).

boundaries were observed in twinned areas as shown by the typical photomicrograph in Fig. 14. In some cases these boundaries were evident at both ends of the twin. In all cases, the boundary followed the trace of a  $(10\bar{1}0)$  plane. Similar boundaries have been reported to occur on  $(11\bar{2}0)$  planes in single crystals of magnesium<sup>(3)</sup>. In that instance however it appears that the crystal under observation was so oriented that the boundary could be attributed to either  $(10\bar{1}0)$  or  $(11\bar{2}0)$  planes. Since numerous boundaries were evaluated here and since in basally cleaved zinc specimens these boundaries are observed to be parallel to twin traces, it appears that this bending of the basal plane is about a  $(10\bar{1}0)$  plane.

Metallographic observations reveal that these low angle boundaries move in conjunction with twin growth. Thus as the twin extends, the accommodation band likewise appears to grow. During bilateral growth the accommodation band increases in width and in angular tilt<sup>(13)</sup>. The reverse mechanisms occurred during detwinning. Thus the existing evidence clearly shows that these low angle boundaries are mobile under stress at atmospheric temperature.

#### NON-CRYSTALLOGRAPHIC LOW ANGLE BOUNDARIES

Another manifestation of the deformation process in hexagonal metals has been the occurrence of forked or curved traces on the surface of grains which have been variously termed rumpling<sup>(5)</sup>, buckling<sup>(5)</sup>, cell formation<sup>(15)</sup>, kinking<sup>(5)</sup>, mosaic walls<sup>(3,13)</sup>, and non-crystallographic low angle boundaries<sup>(14)</sup>. The principal distinction between these low angle boundaries and accommodation boundaries is that the former do not follow well delineated crystallographic planes, are not associated with twinning, and exhibit greater angles of tilt than the accommodation boundaries<sup>(13)</sup>. The genesis of one such boundary (marked A) is shown in Fig. 15. In these



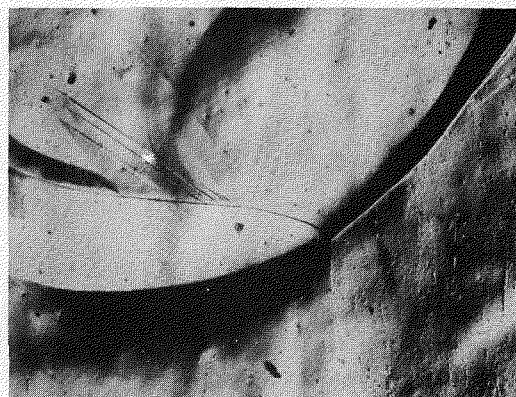
0%  $\epsilon$



0.14%  $\epsilon$



0.35%  $\epsilon$



0.47%  $\epsilon$



0.75%  $\epsilon$



1.06%  $\epsilon$

FIG. 15 THE FORMATION AND MOVEMENT OF A NON-CRYSTALLOGRAPHIC LOW ANGLE BOUNDARY. SPECIMEN 2 (100X REDUCED BY 40%)



figures the stress direction is vertical. On initial straining a general undulation is formed with one terminus at the junction of three grains. On further straining, a sharp non-crystallographic boundary is formed which moves toward the grain boundary as shown by the last three micrographs in Fig. 15. It will also be observed that increased tilting occurs during successive periods of straining. Additional low angle boundaries, B and C, are also formed during straining. Although boundary C appears quite mobile, boundary B does not advance through the accommodation kink emanating from the twin adjacent to the grain boundary. Similar boundaries have been observed in zinc at elevated temperatures<sup>(15)</sup> and it has been suggested that these boundaries are introduced by "drag" during the relative motion of the two adjacent grains. Such a process suggests that the slope of the undulation would be a maximum near the boundary. Although this is consistent with the observation for boundaries B and C, the postulate is not representative for boundary A. It is possible that this boundary might be produced by the nonhomogeneous deformation of grains below the surface. In order to maintain continuity across the grain boundary under the surface, the surface grain is bent and a non-crystallographic boundary is subsequently generated by the appropriate entrapment of like dislocations. Subsequent slip in the grain could cause an increase in the number of trapped dislocations in the vicinity of the boundary thereby not only causing it to move but also to increase the angle of tilt of the boundary. The successive cuts in Fig. 15 reveal that these boundaries are mobile and the angle of tilt does increase with increased straining. This hypothesis is substantiated by such observations as that shown in Fig. 16 where the low angle boundary crosses a grain boundary.

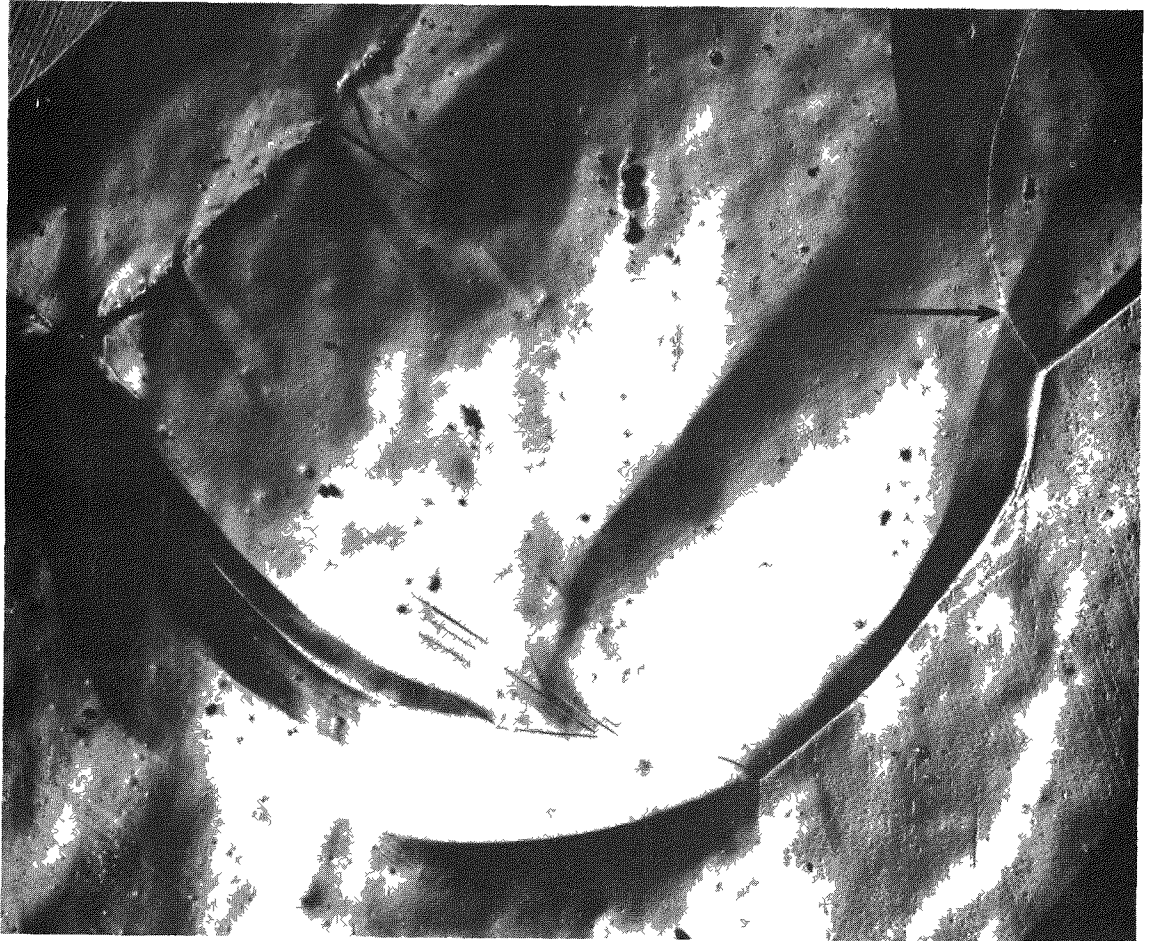


FIG 16 NON-CRYSTALLOGRAPHIC LOW ANGLE BOUNDARY  
OF FIG 15 CROSSING GRAIN BOUNDARY WITH  
NO APPARENT DISCONTINUITY.  
SPECIMEN 2 AT 0.47 %  $\epsilon$ . (100 X REDUCED BY 25%)

Occasionally low angle boundaries appear to originate in the interior of a grain as shown by Figs. 16 and 17, or to start near a grain boundary and traverse from one grain to another with no apparent discontinuity at the grain boundary. Again it appears that the formation of a non-crystallographic boundary might on occasion be caused by nonhomogeneous deformation of underlying grains.

The postulate of bending as a criterion for the formation of a non-crystallographic low angle boundary is consistent with the observations of Pratt and Pugh<sup>(13)</sup>, Jillson<sup>(5)</sup>, and Washburn<sup>(16)</sup>, etc. wherein slight bending readily induces the formation of low angle boundaries. The formation of such boundaries has also been shown to occur on the opposite faces of specimens subjected to mild indentations. Thus the bending can propagate through rather large distances with comparative ease. Indirect evidence is also noted from investigations on single crystals subjected to uniaxial stressing where bending is minimized and the existence of non-crystallographic boundaries is quite rare.

Investigations on the effect of temperature on similar non-crystallographic boundaries in zinc have shown that even prolonged heating in the vicinity of the melting temperature does not cause a change in the shape of these boundaries<sup>(13)</sup>: Although these boundaries are thermally stable, they are quite mobile in stress fields as shown in Fig. 15 for all three non-crystallographic boundaries. In Fig. 18 are recorded the displacements of a number of non-crystallographic boundaries as a function of the applied stress. The displacements were measured approximately normal to the low angle boundary by utilizing etch pits located on each side of the boundary as a traverse for measurement of displacement after successive amounts of strain. Within the limits of experimental accuracy, the boundaries



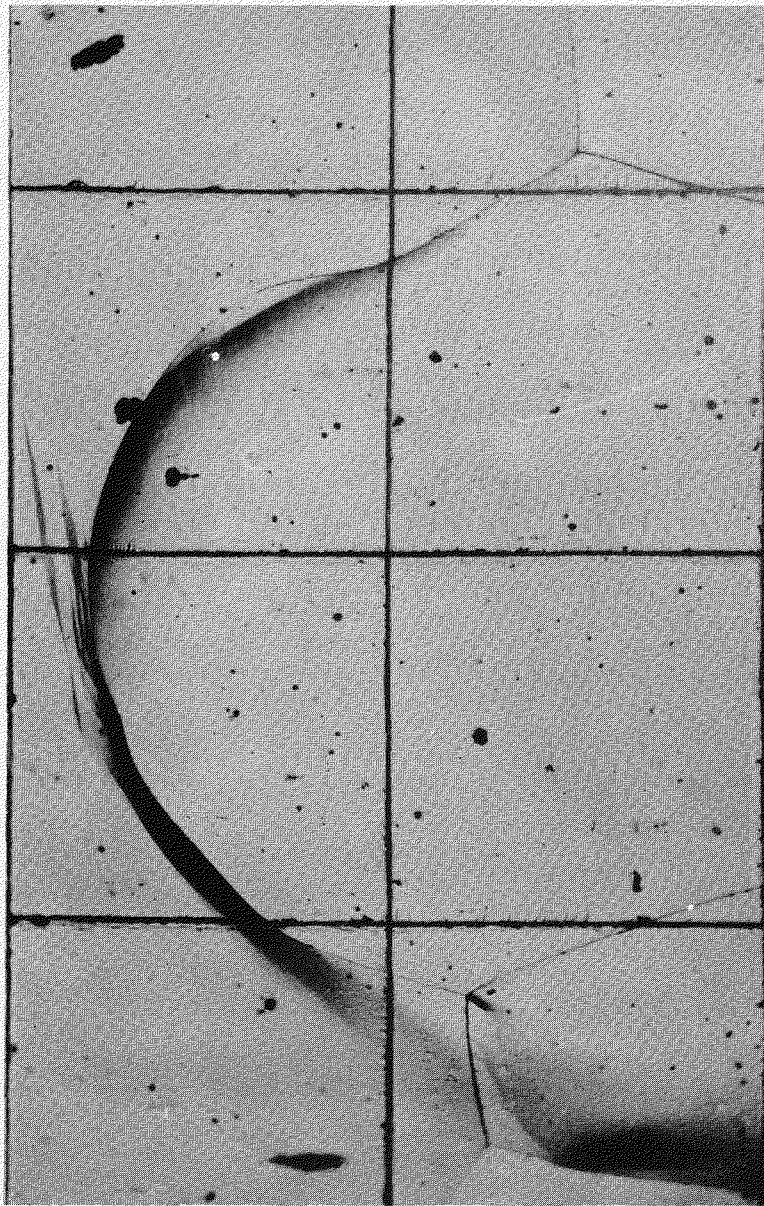


FIG. 17 NON - CRYSTALLOGRAPHIC LOW ANGLE  
BOUNDARY ORIGINATING ALONG GRAIN BOUNDARY.  
SPECIMEN 4 AT 0.52 %  $\epsilon$ . (100X).

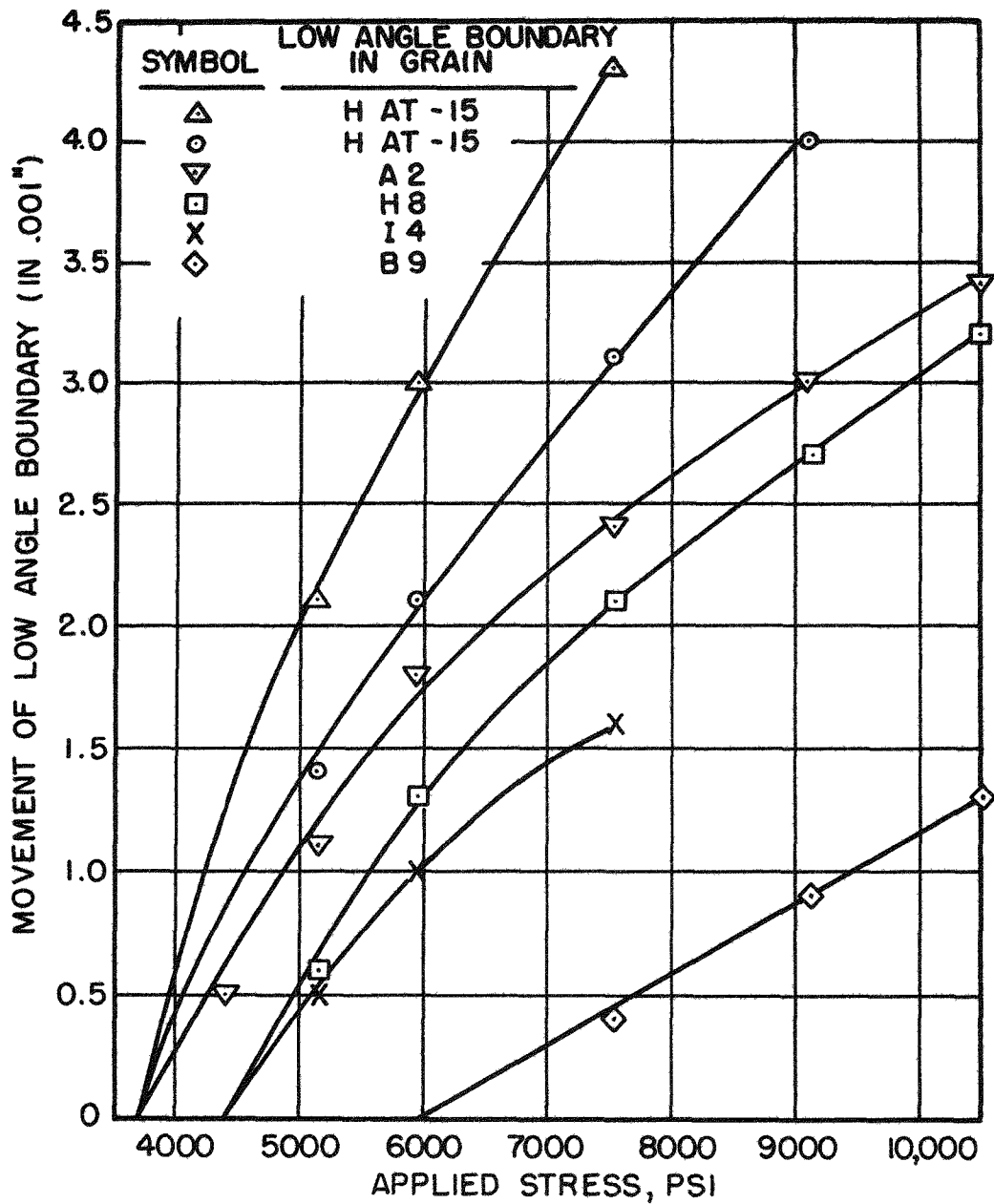


FIG. 18 THE EFFECT OF STRESS ON THE DISPLACEMENT OF NON-CRYSTALLOGRAPHIC LOW ANGLE BOUNDARIES IN MAGNESIUM.

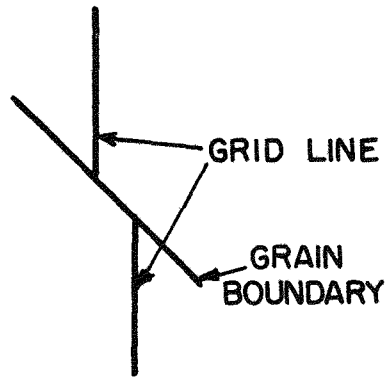
move linearly with the applied stress. Although the boundaries which are approximately at  $45^\circ$  to the stress direction move more readily, in general, than those at either larger or smaller angles, exceptions have been observed.

#### GRAIN BOUNDARY SHEARING

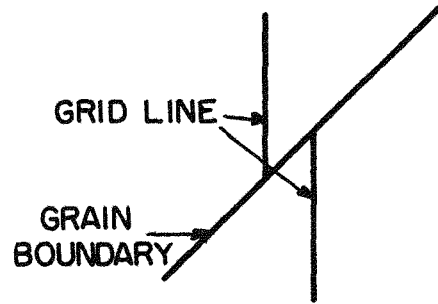
Although grain boundary shearing is quite common in polycrystalline alloys at elevated temperatures, its occurrence at low temperatures, as far as the present authors are aware, has been suggested on only one occasion. Gross<sup>(17)</sup>, during an investigation on the elastic straining of pure iron and silicon iron, observed a rotation of spots on an X-ray pattern during stressing. It could not be deduced, however, whether the slight rotation was attributable to grains or to mosaic subgrains.

In the present investigation, extensive evidence of the existence of grain boundary shearing was observed. At strains as low as 0.16%, shear displacements were observed across the grain boundary between grains L-6 and K-4 in specimen 4 (see Fig. 21). Continued straining caused an increase in the amount of grain boundary shearing in this region as well as the introduction of grain boundary shears in other regions of the specimen. Furthermore the shear was both negative and positive as shown schematically in Fig. 19. Typical examples of both types of shear are recorded in Figs. 20A and B.

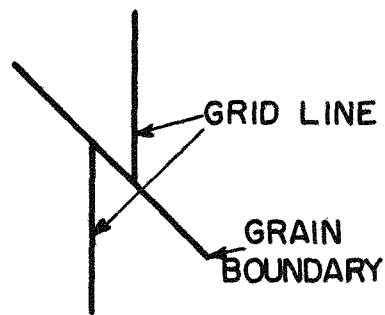
Comparison of the crystal orientations of grains L-6 and K-4 where grain boundary shearing was first observed reveals that both grains have their basal planes essentially parallel to the stress direction and are therefore not suitably oriented for slip. The respective orientations of the two contiguous grains alone, therefore do not appear to offer an explanation for the initiation of grain boundary shear. Examination of



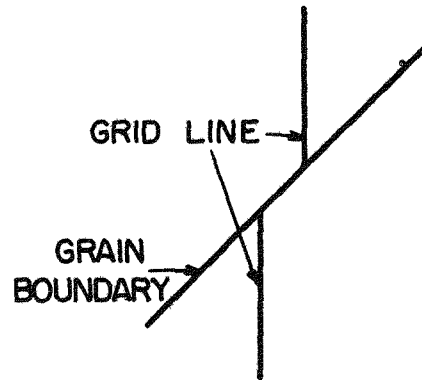
(d) NEGATIVE STRAIN



(b) POSITIVE STRAIN



(c) POSITIVE STRAIN



(d) NEGATIVE STRAIN

FIG. 19 POSITIVE AND NEGATIVE GRAIN BOUNDARY SHEARS. STRESS DIRECTION IS HORIZONTAL.

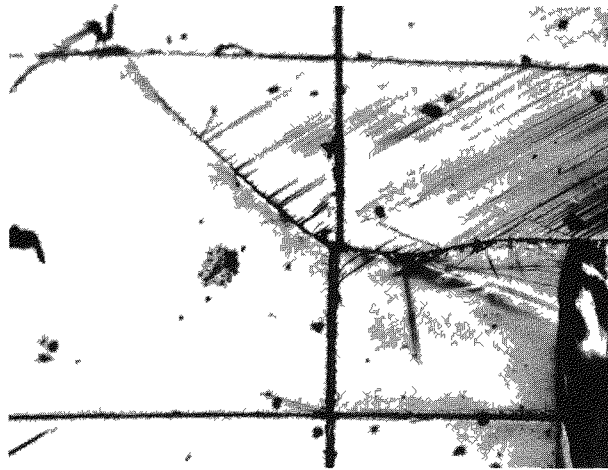


FIG. 20a POSITIVE GRAIN BOUNDARY SHEAR.  
STRESS DIRECTION HORIZONTAL.  
SPECIMEN 3 AT 2.2 %  $\epsilon$  (100X)

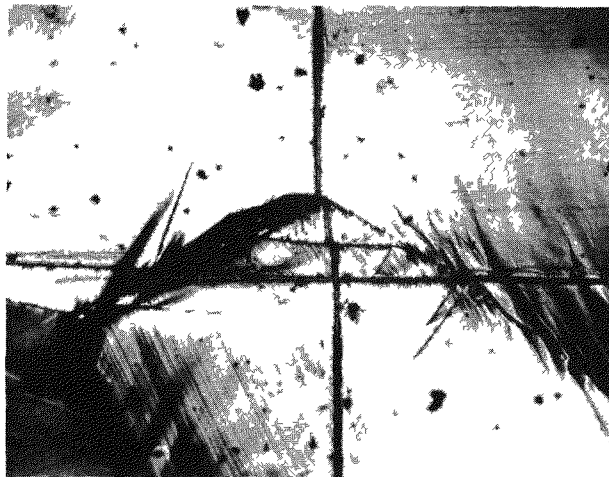


FIG. 20b NEGATIVE GRAIN BOUNDARY SHEAR.  
STRESS DIRECTION HORIZONTAL.  
SPECIMEN 3 AT 2.2 %  $\epsilon$  (100X)



other contiguous grains in Figs. 21A, B and C reveals that both M-2 and J-5 are suitably oriented for slip and do exhibit visible slip as early as 0.16%. During stressing, the stress is relieved in these two grains by plastic deformation, and, perhaps, concentrated in grains K-4 and L-6. The stress concentration thus imposed and the requirement for continuity across the grain boundaries of all grains could lead to the shearing observed. Examination of the upper section of Fig. 21 and Table I reveals a somewhat similar trend in that grains A-6 and D-5 are suitably oriented for slip while grains B-6 and B-9 exhibit relatively low values of  $\sin \chi \cos \lambda$ . Appreciable grain boundary shearing was observed between grains B-6 and B-9. In the center section of Fig. 21 grain boundary shearing between grains F-6 and H-6 is also evident. In this region, F-6 and F-7 are suitably oriented for slip whereas F-4, H-4, H-6 and H-8 are not. Thus grains suitably oriented for slip are located on only one side of those less favorably oriented and may account for the shear between F-6 and H-6 instead of between H-6 and H-8. Again, it is possibly the underlying grains which are responsible for the shear in this case. But in most cases where grain boundary shearing was evident, fracture was also evident. Thus it is possible that fracture precedes grain boundary shearing. In this event, it may be that stress concentration causes premature fracturing which subsequently induces grain boundary shearing to occur. Because of deformation occurring in underlying grains, it is as yet unknown which phenomenon occurs first. The preceding comments are accordingly, apropos for both phenomena.

The total strain contribution from grain boundary shearing was estimated by measuring the displacement across all grain boundaries. The mean displacement per boundary is simply  $\bar{d}_{g.b.}$ . If  $\eta$  grain boundaries

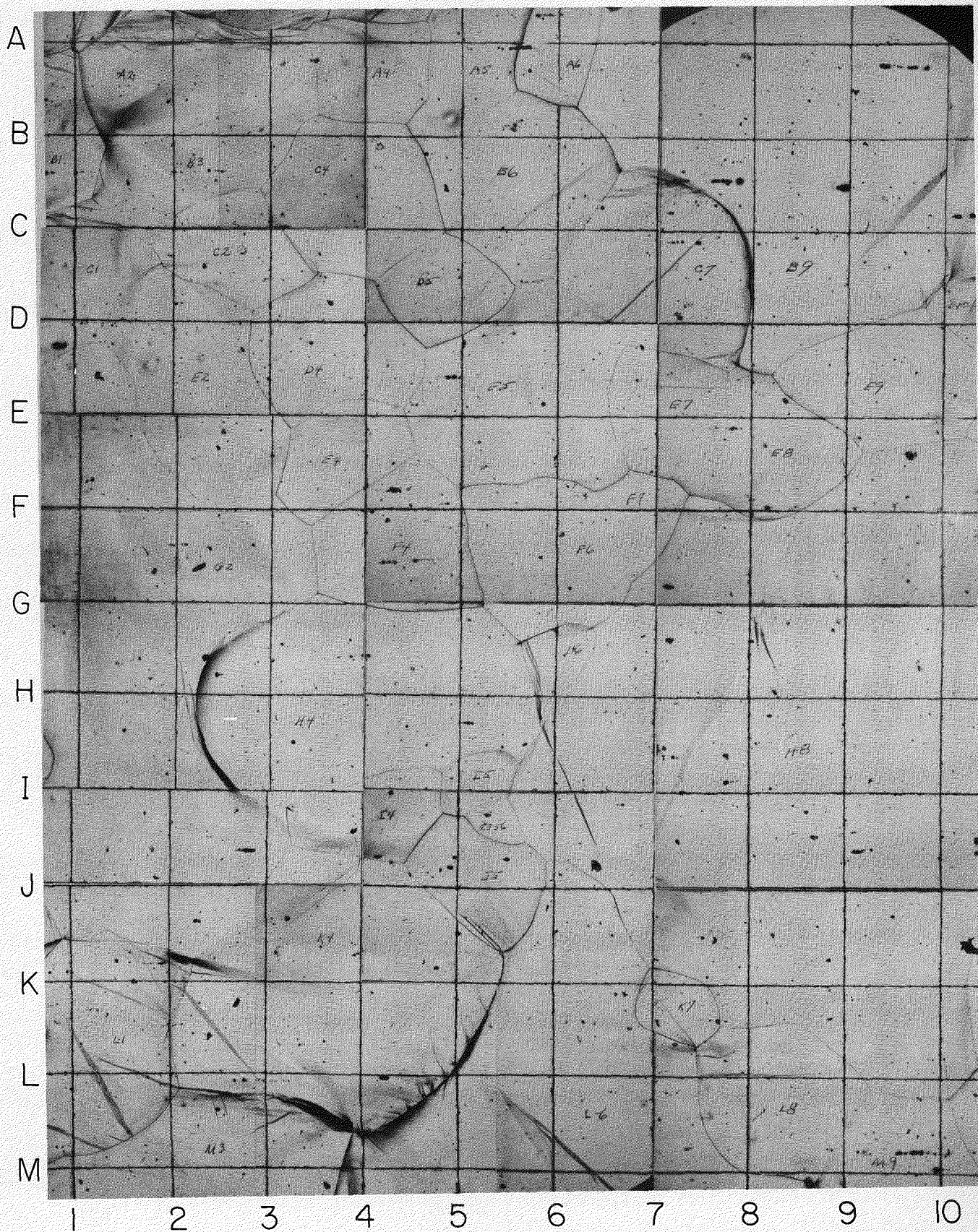


FIG. 21a SPECIMEN 4 AT 0.36%  $\epsilon$ .  
(100X REDUCED BY 70%)



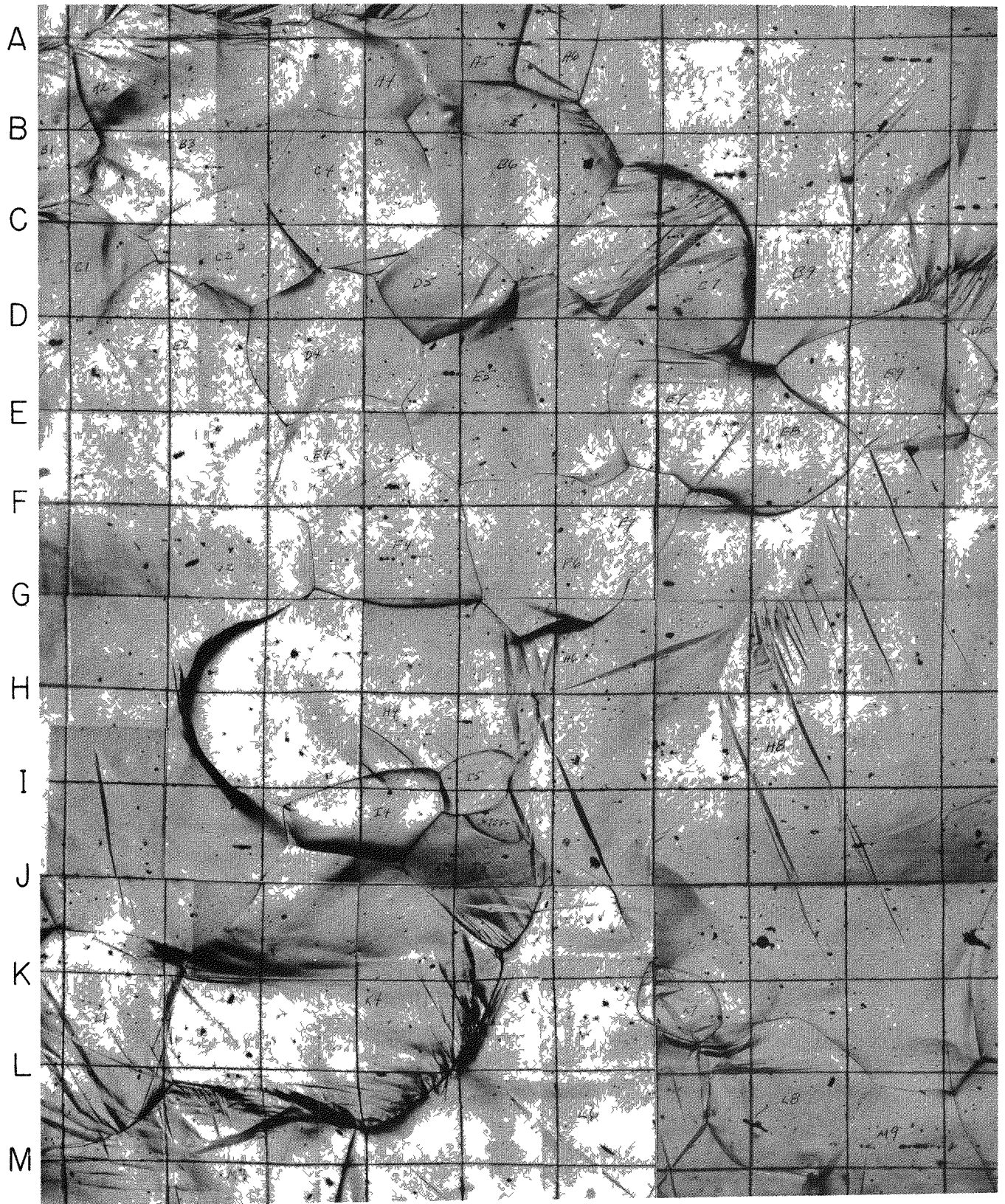


FIG 21b SPECIMEN 4 AT 11%  $\epsilon$   
(100X REDUCED BY 70%)



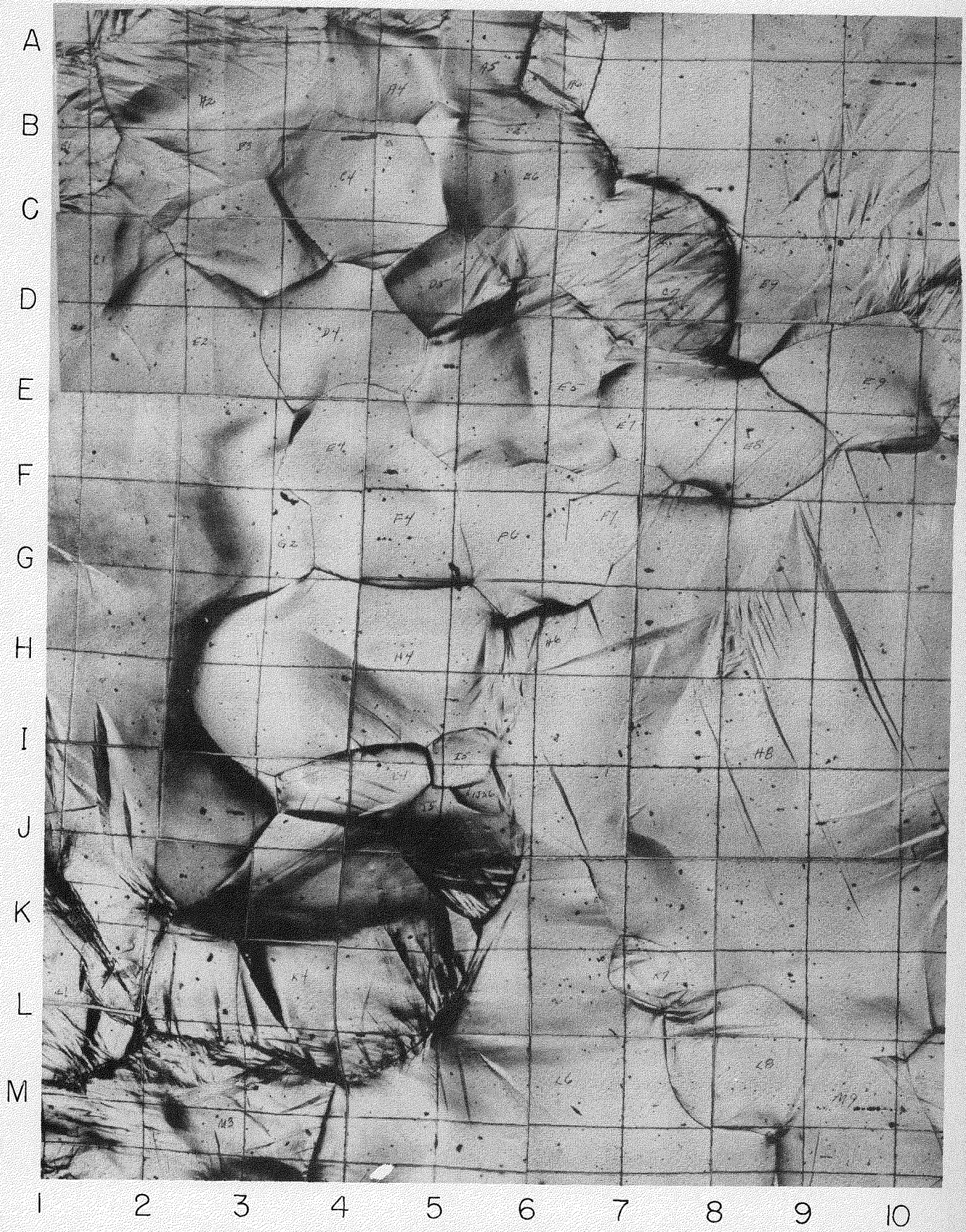


FIG. 21c SPECIMEN 4 AT 3.3%  $\epsilon$ .  
(100X REDUCED BY 70%)

are encountered per unit distance, the strain contribution from grain boundary shearing is

$$\epsilon_{g.b.} = n \bar{d}_{g.b.} \quad (2)$$

Evaluation of  $\epsilon_{g.b.}$  on specimen 4 at a total strain of 2.4% gave a strain of 0.1%. Thus the strain contribution from grain boundary shearing is small. But the effect of grain boundary shearing on subsequent deformation appears large.

Rupturing: In grain K-4 of specimen 4, cracks were first observed at strains as low as 0.16%. The cracks appeared to originate at the grain boundary and grow towards the interior of the grain. Continued straining resulted in additional cracks forming in the same grain which were essentially parallel to the initial ones. Fig. 22, taken at 0.53% strain, reveals 10 of these cracks at an angle of  $60^\circ$  to the stress direction. Subsequent straining produced a second set of major cracks almost normal to the stress direction and a series of finer branched cracks within grain K-4. Concurrently, cracks appeared in both those grains favorably oriented for slip, F-6 and G-2, and those unfavorably oriented - E-7, E-8, B-9, H-8 and L-1.

Orientation determinations of the cracks observed at 100x indicated that the cracks occurred on a number of high index planes such as  $(10\bar{1}9)$ ,  $(20\bar{2}7)$ , etc. But no common orientation of cracks could be obtained for all the cracks visible in specimen 4. The parallelism of the cracks in K-4 shown in Figs. 22 and 23 however suggests an orientation dependence of the cracks. Perhaps alternate shear and cleavage could produce apparent non-crystallographic traces on the surface as shown schematically in Fig. 24. Various combinations of shear displacements and cleavage



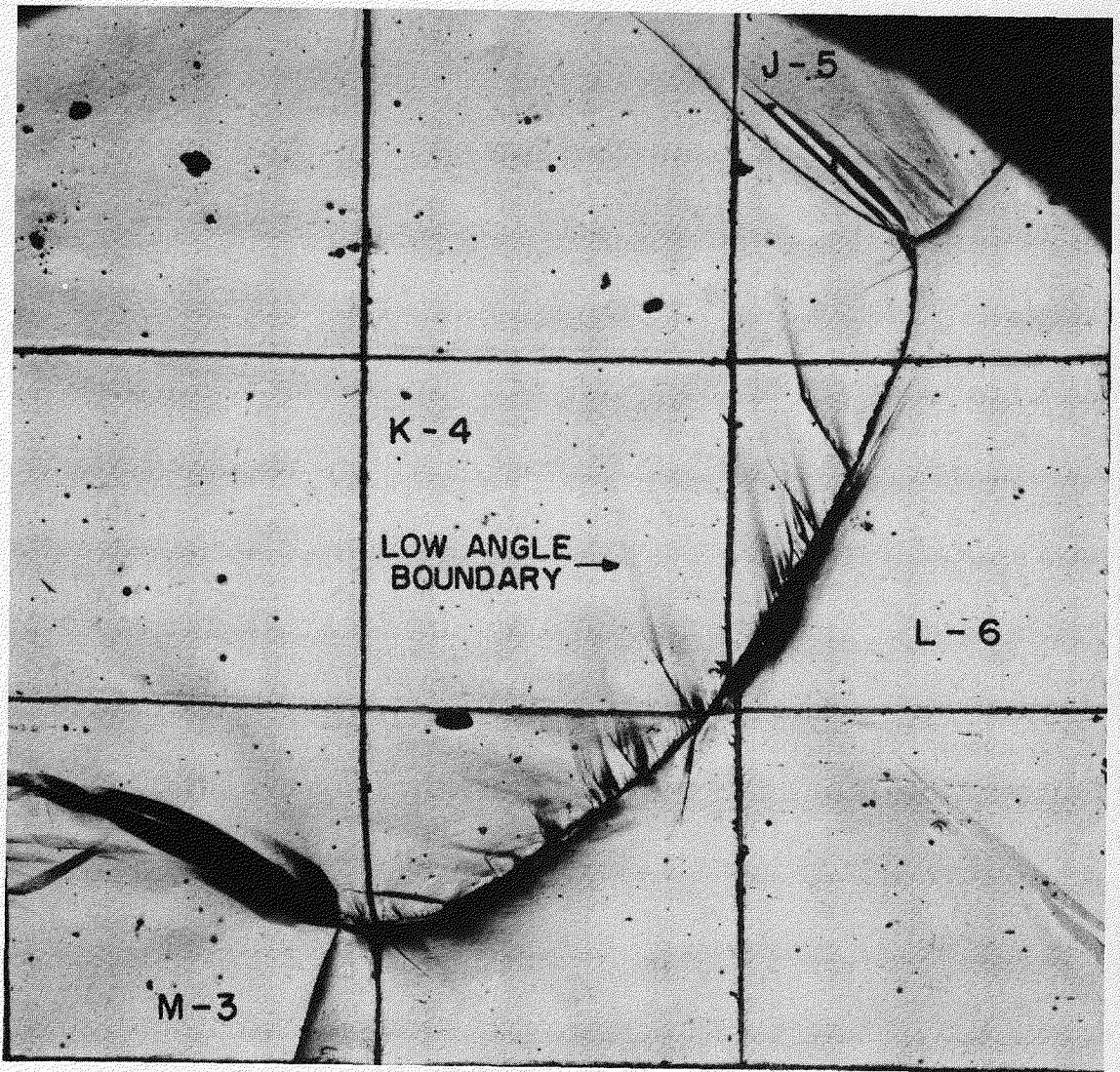


FIG. 22 CRACK FORMATION AT  $60^\circ$  TO STRESS DIRECTION  
IN GRAIN K4 OF SPECIMEN 4 AT 0.53% $\epsilon$ .  
STRESS DIRECTION HORIZONTAL. (100X)



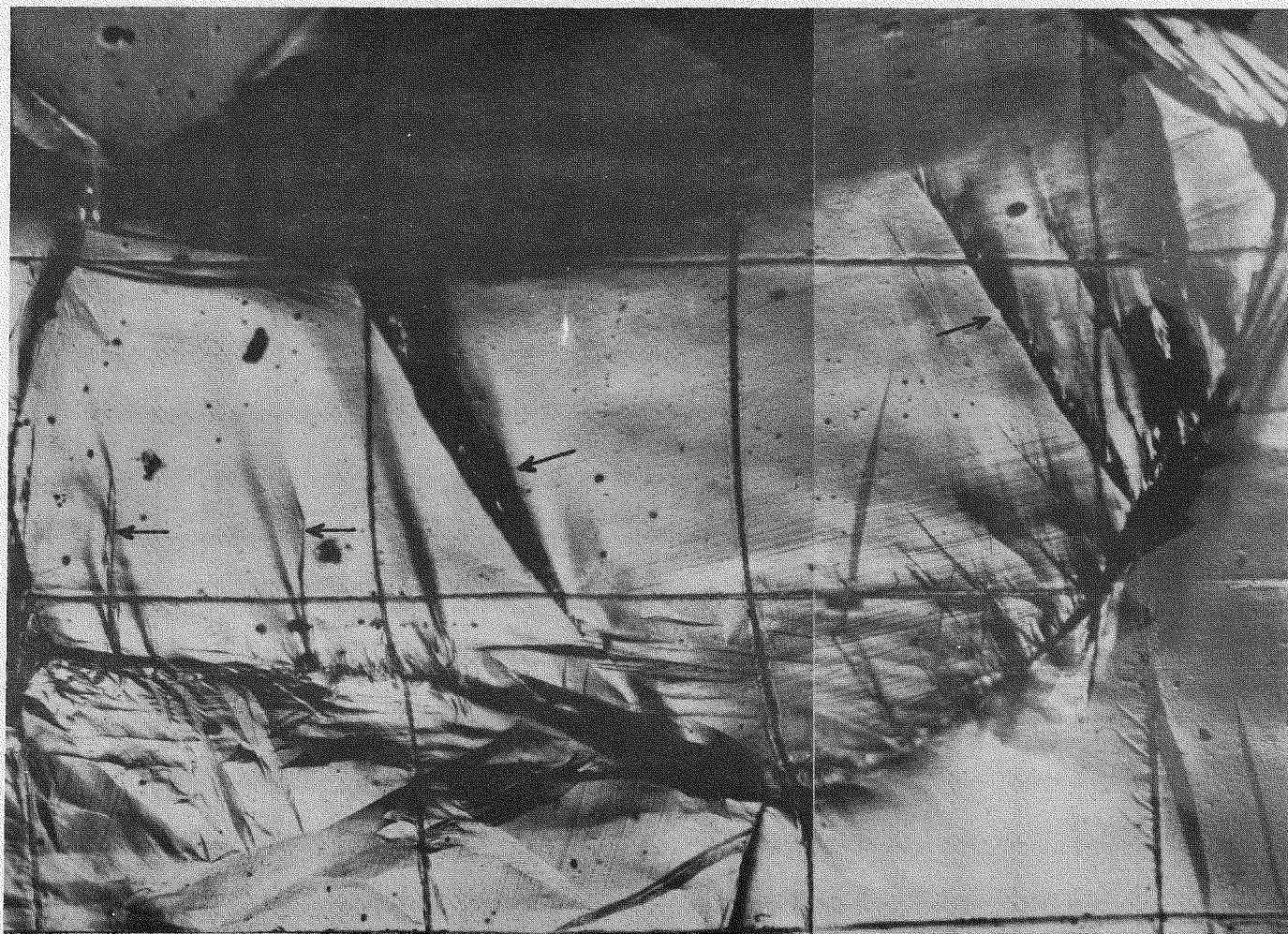


FIG. 23 MAJOR CRACKS IN GRAIN K4 INDICATED BY ARROWS.  
NOTE CRYSTALLOGRAPHIC LOW ANGLE BOUNDARIES ASSOCIATED  
WITH CRACKS. SPECIMEN 4 AT 2.4 %  $\epsilon$ .  
(100X)



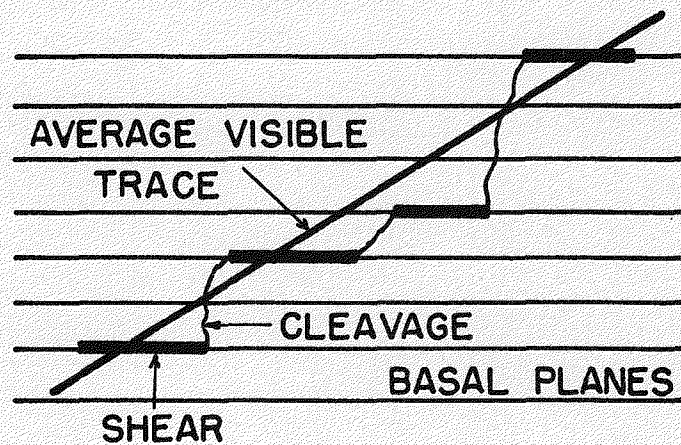


FIG. 24 ALTERNATE SHEAR ON BASAL PLANE AND CLEAVAGE OR TEARING WHICH RESULTS IN NON-CRYSTALLOGRAPHIC MICROCRACKS IN SPECIMEN. (SPECIMEN SURFACE IN PLANE OF PAPER.)

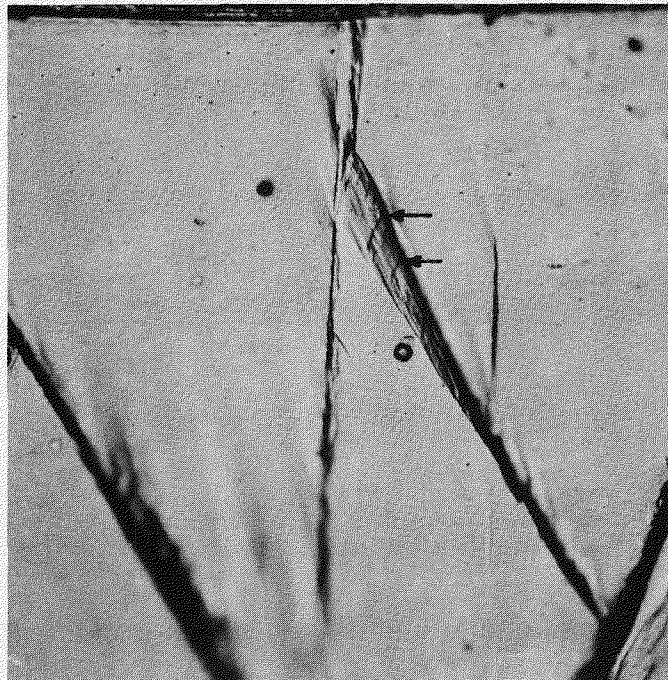


FIG. 25 PARALLEL CLIFFS ON FACE OF CRACKS IN GRAIN K 4. SPECIMEN 4 AT 0.71 %  $\epsilon$ . (500X).

would thus yield non-crystallographic surface traces. Moreover, these traces would be more or less parallel in any one grain but could alter appreciably from grain to grain due to interaction between conjugate grains. Qualitative validity for this postulate is given in Fig. 25 which shows one of the cracks in grain K-4 at 500x. Here it is noted that parallel, sharp, cleavage-like cliffs are present in the crack. Between these cleavage-like cliffs appears the rough dull surface indicative of shear fractures. Since the surface of the crack is inclined to the surface of the specimen, a true orientation of the facets on the crack cannot be obtained. It was estimated, however, that they correspond to  $(10\bar{1}1)$  traces.

It is interesting to note that crystallographic low angle boundaries are evident at the tip of the cracks and have the same orientation  $(10\bar{1}0)$  as the accommodation boundaries associated with twinning. Qualitative evaluation of the surface contour on both sides of the cracks revealed that the low angle boundaries always occurred on the depressed side of the crack. Typical examples are shown in Figs. 22 and 23 for the cracks in grain K-4. The shear displacement along the crack and downward in the grain, as shown in Fig. 25, gives rise to the same geometrical relationship shown for twinning in Fig. 13. In this case the twin can be replaced by the crack. Thus, it appears that the basal plane is bent by the formation of cracks in much the same manner as in the formation of a twin.

The final rupture of specimen 4 occurred primarily by intergranular fracture of grains whose boundaries were approximately at  $45^\circ$  to the direction of stressing in such a manner that a macroscopic "saw tooth" rupture normal to the stress direction was obtained. This region was outside of the section selected a priori for study. But it was interesting

to note that a second intergranular rupture started in grain L-1 and followed the grain boundary of grain G-2 (just off the diagram shown in Fig. 21). This failure extended across approximately 3/4 of the specimen.

#### CONCLUSIONS

1. Polycrystalline magnesium was observed to slip exclusively by the mechanism  $(0001) [10\bar{1}0]$  at room temperature.
2. Twinning occurred exclusively along the  $(10\bar{1}2)$  planes.
3. Low angle kink boundaries issuing from the spurs of mechanical twins were found to agree with the hypothesis that they consist of a series of edge dislocations on  $(10\bar{1}0)$  planes.
4. Grain boundary shearing was observed at room temperature.
5. Non-crystallographically oriented low angle boundaries were produced during deformation of polycrystalline aggregates of magnesium.
6. Rupturing occurred on a number of high order crystallographic planes as well as along the grain boundaries.

#### ACKNOWLEDGMENT

This investigation was conducted under sponsorship of the Office of Ordnance Research. The authors express their sincere appreciation to the O.O.R. for their wholehearted support of this investigation.



REFERENCES

1. E. Schmid, "Bertrage Zur Physik und Metallographie des Magnesium", Zeit. fur Electrochemie, vol. 37, 1931, p. 447.
2. E. C. Burke and W. R. Hibbard, Jr., "Plastic Deformation of Magnesium Single Crystals", Trans. AIME, vol. 194, 1953, p. 295.
3. Dow Chemical Co., "Plasticity of Magnesium Alloy Single Crystals and Origin of Secondary Maxima (002) Pole Figures for Rolled Magnesium Alloys", Final Report No. 15960, Part 2, 1953, pp. 10-11.
4. Dow Chemical Co., Part 3, p. 18, *ibid.*
5. D. C. Jillson, "An Experimental Survey of Deformation and Annealing Processes in Zinc", Trans. AIME, vol. 188, 1950, p. 1009.
6. C. H. Mathewson and A. J. Phillips, "Twinning in Be, Mg, Zn, and Cd", Trans. AIME, 1928, p. 445.
7. E. Schiebold and G. Siebel, "Studien an Magnesium und Magnesium Legierungen", Zeit. fur Physik, vol. 69, 1931, p. 458.
8. J. E. Dorn and E. Thomsen, "Magnesium, Notes on the Modulus of Elasticity", Light Metal Age, vol. 1, 1943, p. 10.
9. N. Thompson and D. J. Millard, "Twin Formation in Cd", Phil. Mag. vol. 43, 1952, p. 422.
10. N. N. Davidsen, A. F. Kolesnikov, and K. V. Fedoriv, J. Exp. Theor. Physic. USSR 3, 1933, p. 350.
11. R. F. Miller, "Creep and Twinning in Zinc Single Crystals", Trans. AIME, vol. 122, 1936, p. 176.
12. P. A. Bakarian and C. H. Mathewson, "Slip and Twinning of Magnesium Single Crystals at Elevated Temperatures", Trans. AIME, vol. 152, 1943, p. 226.
13. P. L. Pratt and S. F. Pugh, "The Movement of Twins, Kinks and Mosaic Walls in Zinc", Acta Metallurgica, vol. 1, No. 2, March 1953, p. 218.
14. F. E. Hauser, C. D. Starr, L. Tietz, and J. E. Dorn, "Deformation of Polycrystalline Magnesium Alloy", First Status Report, University of California, Inst. of Engineering Research, Report Series No. 73, Issue No. 1, Sept. 15, 1953.
15. R. C. Gifkins and J. W. Kelley, "Note on the Formation and Development of Cells in Polycrystalline Zinc", Acta Metallurgica, vol. 1, May 1953, p. 320.
16. C. H. Li, E. H. Edwards, J. Washburn, and E. R. Parker, "Stress Induced Movement of Crystal Boundaries", Acta Metallurgica, vol. 1, No. 2, March 1953, p. 223.

17. N. P. Gross, "Grain Displacement in Metal Stressed below Elastic Limit" Metals Progress, vol. 61, 1952, p. 87.
18. A. B. Greninger, "Determination of Orientations of Metallic Crystals by Means of Back-Reflection Laue Photographs", Trans. AIME, vol. 117, 1935, p. 61.
19. E. I. Salkovitz, "Crystallographic Angles for Magnesium, Zinc and Cadmium", Trans. AIME, vol. 189, 1951, p. 64.
20. C. S. Barrett, "Structure of Metals", McGraw-Hill Co., N.Y., 1943.

APPENDIX

ORIENTATION DETERMINATIONX-Ray Procedure

Laue back-reflection photographs were taken of the polished magnesium tensile specimen using a tungsten target operated at 50 KV. and 16 ma. A small pinhole (relative to grain diameter) of 0.3 cm diameter was used with a film to specimen distance of 3 cm. Exposure times were  $1\frac{1}{2}$  hours on double emulsion X-ray film.

In order to determine that the X-rays impinged on the appropriate grain in the polycrystalline aggregate, a telescope, whose optical axis had been aligned with the X-ray beam by trial and error correction, was mounted on an auxiliary track of the X-ray unit. After the appropriate grain in the specimen had been brought into coincidence with the cross hairs of the telescope, the specimen holder was transferred to the track on the X-ray unit and an appropriate exposure made.

Reduction of X-ray Data

The interpretation of the X-ray photograph was carried out by making use of the chart developed by Greninger<sup>(18)</sup> together with a stereographic net (Wulff net) and a standard projection of Mg<sup>(19)</sup>. The procedure of converting the X-ray data into a stereographic projection is outlined in "Structure of Metals" by Barrett<sup>(20)</sup> and will not be repeated here.

The angle  $\chi$  between the tension axis and the (0001) pole and the angle  $\lambda$  between the tension axis and the most favorably oriented  $[11\bar{2}0]$  direction for slip could be measured directly from the stereographic projection.

The direction of the traces of the slip planes in Fig. 1 were determined by inscribing a line at  $90^\circ$  to the one joining the center of the projection to the (0001) pole. Thus the angle between the slip trace and stress direction could readily be measured.

DETERMINATION OF CRYSTAL ORIENTATION FROM TRACES ON A SURFACE

The crystal orientation can be determined if sufficient traces are evident on the surface and the kinematics are known for the deformation process responsible for these traces. Or, conversely, the kinematics of a trace can be deduced if the crystal orientation is known. By measuring the angle between the stress direction and the surface trace, the locus of the possible poles of the trace on the photomicrograph can be determined. These loci form diameters on a stereographic projection. By trial and error the standard projection can be rotated such that all poles causing traces (such as  $(10\bar{1}2)$  twin plane poles) fall on their respective loci after an equal amount of rotation. This rotated standard projection represents the actual crystal orientation of the grain studied. Conversely, if the orientation of the crystal is known, some standard pole will rotate on to the locus determined by measuring the angle between the trace and stress direction. This is the pole of the plane whose intersection with the plane of polish caused the trace. Often, however, a number of solutions will be obtained. By analyzing a number of grains, it is often possible to determine the plane which was operative in producing the surface trace. For example, the low angle boundaries associated with twinning were always found to occur on  $(10\bar{1}0)$  planes. Moreover, the  $(10\bar{1}0)$  pole of the bend plane was always observed to belong to the same major zone as the associated  $(10\bar{1}2)$  twin plane. In the case of cracks in the present investigation no common solution was found for each type of trace, and it was concluded, therefore, that the traces were non-crystallographic.

COMPONENT OF STRAIN BY TWINNING

It has been shown<sup>(20)</sup> that the strain attending twinning can be calculated from

$$\epsilon_{TW} = \frac{l}{l_0} - 1 = \sqrt{1 + 2\delta \sin \chi' \cos \lambda' + \delta^2 \cos^2 \chi'} - 1 \quad (3)$$



where  $l_0$  = initial length  
 $l$  = final length  
 $\gamma$  = shear strain on twinning = 0.131 for Mg where  $\gamma = 1.624$   
 $\chi'$  = angle between twin plane and stress direction  
 $\lambda'$  = angle between twin direction and stress direction.

The iso-strain lines of tensile stress directions for twinning on plane I are shown on the right hemisphere of the standard stereographic projection in Fig. 37. For a given stress direction (values of  $\chi'$  and  $\lambda'$ ) the shear strain on twinning can be determined directly from this figure. Fig. 11 in the report is a simplified version of Fig. 37 indicating only whether the strain is positive or negative on twinning.

#### SHEAR STRESS FOR TWINNING

If twinning is a stress phenomenon and obeys a law similar to that for slip, then

$$\sigma_{CT} = \sigma_T \sin \chi' \cos \lambda' \quad (4)$$

where  $\sigma_T$  = stress for twinning  
 $\sigma_{CT}$  = critical shear stress for twinning  
 $\chi'$  = angle between twin plane and stress direction  
 $\lambda'$  = angle between twin direction and stress direction.

In the left hemisphere of Fig. 37 are recorded the lines of equal critical shear stress on the twinning plane for a tensile stress of one psi. No critical shear stress for twinning could be determined in this investigation and the validity of equation (4) is doubtful.

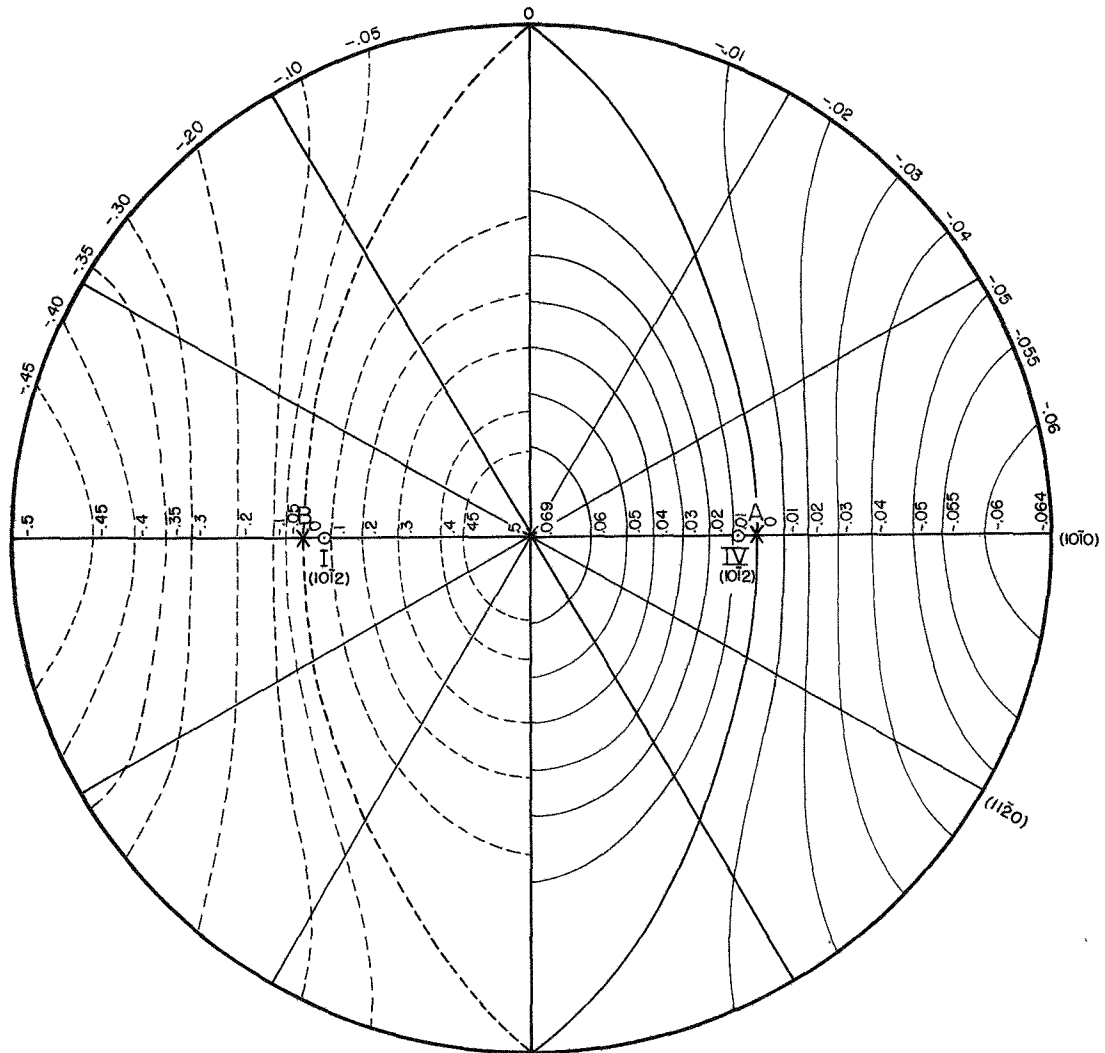


FIG. 37A LEFT HEMISPHERE

$$\sigma_{CT} = \sigma_T \sin \chi^I \cos \lambda^I$$

WHERE:  $\sigma_T$  = TENSILE STRESS FOR TWINNING.  
 $\sigma_{CT}$  = CRITICAL SHEAR STRESS FOR TWINNING.

$\chi^I$  = ANGLE BETWEEN TWIN PLANE AND STRESS DIRECTION.

$\lambda^I$  = ANGLE BETWEEN TWIN DIRECTION AND STRESS DIRECTION.

PLOT OF  $\sin \chi^I \cos \lambda^I$  FOR TWINNING ON PLANE IV IN DIRECTION B.

FIG. 37B RIGHT HEMISPHERE

$$\epsilon_{TW} = \sqrt{1 + 2 \bar{\sigma} \sin \chi^I \cos \lambda^I \bar{\sigma}^2 \cos^2 \chi^I - 1}$$

WHERE:  $\epsilon_{TW}$  = STRAIN ON TWINNING.  
 $\bar{\sigma}$  = SHEAR STRAIN ON TWINNING. (0.131 FOR Mg.)

$\chi^I$  = ANGLE BETWEEN TWIN PLANE AND STRESS DIRECTION.

$\lambda^I$  = ANGLE BETWEEN TWIN DIRECTION AND STRESS DIRECTION.

PLOT OF  $\epsilon_{TW}$  AFTER TWINNING ON PLANE I IN DIRECTION A.

TECHNICAL REPORT DISTRIBUTION LIST

1. Office of Ordnance Research Box CM, Duke Station Durham, North Carolina	- 10	15. Chief, Ordnance Development Div. National Bureau of Standards Washington 25, D. C.	- 1
2. Office, Chief of Ordnance Washington 25, D. C. Attn: ORDTA	- 1	16. Commanding Officer Watertown Arsenal Watertown 72, Mass.	- 2
3. Office, Chief of Ordnance Washington 25, D. C. Attn: ORDTB	- 1	17. Technical Reports Library SCEL, Evans Signal Corps Lab. Belmar, New Jersey	- 1
4. Office, Chief of Ordnance Washington 25, D. C. Attn: ORDTR	- 1	18. Commanding Officer Engineer Res. & Dev. Laboratories Fort Belvoir, Virginia	- 1
5. Office, Chief of Ordnance Washington 25, D. C. Attn: ORDTS	- 1	19. Commander U. S. Naval Proving Ground Dahlgren, Virginia	- 1
6. Office, Chief of Ordnance Washington 25, D. C. Attn: ORDTT	- 1	20. Chief, Bureau of Ordnance (AD3) Department of the Navy Washington 25, D. C.	- 1
7. Office, Chief of Ordnance Washington 25, D. C. Attn: ORDTU	- 1	21. U.S. Naval Ordnance Laboratory White Oak, Silver Spring 19, Md. Attn: Library Division	- 1
8. Office, Chief of Ordnance Washington 25, D. C. Attn: ORDTX (Tech. Library)	- 1	22. Director National Bureau of Standards Washington 25, D. C.	- 1
9. Office, Chief of Ordnance Washington 25, D. C. Attn: ORDTX-P	- 1	23. Corona Laboratories National Bureau of Standards Corona, California	- 1
10. Commanding General Aberdeen Proving Grounds, Md. Attn: BRL	- 1	24. Commanding Officer Frankford Arsenal Bridesburg Station Philadelphia 37, Penna.	- 2
11. Commanding Officer Redstone Arsenal Huntsville, Alabama	- 1	25. Technical Information Service P. O. Box 62 Oak Ridge, Tennessee Attn: Reference Branch	- 1
12. Commanding Officer Picatinny Arsenal Dover, New Jersey	- 1	26. Commanding Officer Signal Corps Engineering Lab. Fort Monmouth, New Jersey Attn: Director of Research	- 1
13. Commanding Officer Rock Island Arsenal Rock Island, Illinois	- 1	27. The Director Naval Research Laboratory Washington 25, D. C. Attn: Code 2021	- 1
14. Commanding General Research & Engineering Command Army Chemical Center, Md.	- 1		

TECHNICAL REPORT DISTRIBUTION LIST

- |  |  |
|--|--|
| 28. Jet Propulsion Laboratory<br>California Institute of Technology<br>4800 Oak Grove Drive<br>Pasadena 3, California - 1                    | 38. Commanding General<br>Air Material Command<br>Wright-Patterson Air Force Base<br>Dayton 2, Ohio<br>Attn: F.N. Bubb, Chief Scientist<br>Flight Research Lab. - 1                        |
| 29. Director, Applied Physics Lab.<br>Johns Hopkins University<br>8621 Georgia Avenue<br>Silver Spring 19, Maryland - 1                      | 39. Office of the Chief Signal Officer<br>Engineering & Technical Division<br>Engineering Control Branch<br>Room 2B273, Pentagon Bldg.<br>Washington 25, D. C.<br>Attn: SIGGD - 1          |
| 30. Chief, San Francisco Ordnance District<br>1515 Clay Street<br>Oakland 12, California - 3   | 40. NAC for Aeronautics<br>1724 F Street, NW<br>Washington 25, D. C.<br>Attn: Mr. E.B. Jackson, Chief,<br>Office of Aeronautical<br>Intelligence - 1                                       |
| 31. Commanding General<br>Air University<br>Maxwell Air Force Base, Alabama<br>Attn: Air University Library - 1                              | 41. Scientific Information Section<br>Research Branch<br>Research & Development Division<br>Office, Assistant Chief of Staff,<br>G-4<br>Department of the Army<br>Washington 25, D. C. - 1 |
| 32. Document Service Center<br>U.B. Building<br>Dayton 2, Ohio<br>Attn: DSC-SD - 1   |  |
| 33. Commanding General<br>Air Res. & Dev. Command<br>P. O. Box 1395<br>Baltimore 3, Maryland<br>Attn: RDD - 1                                |  |
| 34. Commanding General<br>Air Res. & Dev. Command<br>P. O. Box 1395<br>Baltimore 3, Maryland<br>Attn: FDR - 1                                |  |
| 35. Chief of Naval Research<br>c/o Reference Department<br>Technical Information Division<br>Library of Congress<br>Washington 25, D. C. - 3 |  |
| 36. Commander<br>U.S. Naval Ord. Test Station,<br>Inyokern<br>China Lake, California<br>Attn: Technical Library - 1                          |  |
| 37. U.S. Atomic Energy Commission<br>Document Library<br>19th & Constitution Avenue<br>Washington 25, D. C. - 1                              |  |